


Coupled extensional-flexural vibration behaviour of a system of elastically connected functionally graded micro-scale panels

K.B. Mustapha* 

Faculty of Engineering, Computing and Science, Swinburne University of Technology (Sarawak Campus), Jalan Simpang Tiga, 93350 Kuching, Sarawak, Malaysia

This study is concerned with the free vibration behaviour of a system of elastically connected functionally graded micro-scale panels. The mechanical properties of the micro-panel are assumed to have a through-thickness variation and governed by a power-law relation in terms of the constituents' volume fractions. The biharmonic equations governing the motion of each micro-panel are formulated through the adoption of the energy method along with the postulates of the Kirchhoff–Love plate theory. Concentrating on the asynchronous motion of the connected micro-panels, the study investigates the shift of the natural frequencies of the system as a result of variation in the: aspect ratio of the micro-panel, span-to-thickness ratio of the micro-panel; gradient index; small-scale effect; and the ratio of the Young's modulus. Estimates of the natural frequencies, under the assumption of simply-supported edges of the micro-panels, are provided by the Navier's solution method. The qualitative assessment of the model's parameters indicates that the effect of the gradient index is stifled by the presence of the size effect. Moreover, it is observed that higher values of the ratio of the constituents' Young's modulus generate a stiffer response of the micro-panel than higher values of the connectors' stiffness and the constituents' density ratio.

Keywords: functionally graded plate; modified couple stress; vibration; size effect

1. Introduction

Recent decades have witnessed sustained research studies that are tailored to the accurate prediction of the electrical, magnetic and mechanical response of small-scale structural elements, most of which contribute to the development of microelectromechanical and nanoelectromechanical systems (MEMs and NEMS). A good number of these studies have identified application areas where the small-scale footprints of MEM and NEM systems find competitive usage to include chemical sensing, mass detection, actuation and microwatt force transmission in artificial skeletal muscle (Li & Su, 2010; Saliterman, 2006). Additionally, notable devices where micro-sized structural elements (such as ultra-thin film, micro-scale plate and micro-scale beam, ultra-thin transmission wire) provide unalloyed advantage include portable field accelerometers, electrical filters, gyroscopes, hydrophones, high-Q oscillators, bioassay microfluidic networks (for patterned drug delivery) and inertia sensors (Kun & Nguyen, 1999; Mattila et al., 2002; Nguyen, 1995; Yazdi, Ayazi, & Najafi, 1998).

A common feature of micro-structural elements is the possession of microns or sub-microns dimension over their cross-sectional geometry. From past research studies,

*Email: kbmustapha@swinburne.edu.my

evidence have been provided for the correlation between the response of these micro-structural elements and their material length scale. This observed correlation leads to the detection of the fact that as the thickness of these structures become menacingly close to the internal material length scale parameter, the phenomenon of size effect sets in and consequently affects the response of the structures (Fleck & Hutchinson, 1993; Thai & Vo, 2013). It is in this spirit that, for the optimal design of micro and nano-sized structures, adopting the classical continuum theory is not an option, since the theory falls short in the prediction of the contribution of size effect to the mechanical behaviours of these delicate structures. Accordingly, a stellar array of studies has been reported on the quest to address the significance of size effect in microstructured materials through the so-called enriched continuum mechanics (Challamel, 2013; Thai & Uy, 2013). Essentially, the formulations of these enriched continuum theories build on the theoretical foundation laid down, over a century ago, by the Cosserat brothers (Cosserat, 1909).

Closer to our time, studies on size-dependent behaviour of microstructured materials yield by the enriched continuum theories keep growing. For example, starting from the 1960s, the works of Mindlin (Mindlin & Tiersten, 1962) and Toupin (1964) advanced the concept of couple stress theory so as to account for size effect in microstructured materials. Additional progress was made between the 1980s and 1990s when Aifantis (1984, 1992) and Fleck and Hutchinson (1993); Fleck, Muller, Ashby, and Hutchinson, (1994) expounded the idea of strain gradient theory in plasticity. Meanwhile, a well-founded difficulty with these theories is the inability to determine the resultant microstructure-dependent material constants, as explained in Lam, Yang, Chong, Wang, and Tong (2003), Maranganti and Sharma (2007) and Reddy (2011). Consequently, models of the structural elements with one or at most two length scale parameter(s) offer experimental benefit and mathematical convenience. The modified couple stress theory (MCST), which is adopted in the current study, is one such higher order elasticity theories in which the characterisation of size effect is done with just one material length scale parameter (Papargyri-Beskou, Tsepoura, Polyzos, & Beskos, 2003; Yang, Chong, Lam, & Tong, 2002). The MCST has already set off a burst of research activities in the theoretical prediction of the deformational response of micro-scale structural elements. Initial application of the MCST focused on the analyses of homogeneous micro-scale beams, rods and micro-scale pipes (Anthoine, 2000; Akgöz & Civalek, 2013; Mustapha & Zhong, 2012a, 2012b; Park & Gao, 2006; Reddy, 2011; Wang, Liu, Ni, & Wu, 2013). However, a very limited number of recent studies have extended the work to the analyses of two-dimensional micro-scale plates (Abbasi & Mohammadi, 2013; Akgöz & Civalek, 2013; Gao, Huang, & Reddy, 2013; Jomehzadeh, Noori, & Saidi, 2011; Sharma & Kumar, 2013; Yin, Qian, Wang, & Xia, 2010).

It is known that the design of new structures and systems with enhanced mechanical properties remains a major driver for the investigation of advanced materials. Indeed, the last few decades have seen the use of advanced materials in a wide range of engineering applications. Prominent among these advanced materials are the functionally graded materials (FGMs) (Şimşek, Kocatürk, & Akbaş, 2012; Sur & Kanoria, 2014). FGMs have been specifically recognised as a potential solution to some of the challenging problems associated with the conventional laminate composite. The idea of FGMs was first introduced in 1984 by Japanese material scientists (Koizumi, 1992). Suitably exploited, structures made of FGMs have been reported, experimentally and theoretically, to yield substantial improvement in performance, especially in applications that require reduction of maximum principal tensile stress in bulk materials (Choi

et al., 2010). FGMs offer high thermal resistance, high fracture toughness and represent a viable way to minimise the propagation of Hertzian cracks (Choi et al., 2010). Structural elements made of FGMs that have found usage include the design of wear-resistant linings, rocket heat shields, biomedical and optical devices (Boss & Ganesh, 2006; Shaw, 1998; Suresh & Mortensen, 1997).

Drawing on the rising importance of FGMs in the design of micro-scale devices, past studies have touched on the need for thorough examination of the behaviour of structures made of FGMs under different mechanical loads. This has led to the emergence of studies that are directed towards the investigation of the influence of the inhomogeneity generated by the functional gradation on the response of structural elements (Daouadji, Henni, Tounsi, & El Abbes, 2013; Mohammadi, Saidi, & Jomehzadeh, 2010). Technically, investigations of the influence of material inhomogeneity on the response of structures dates back to more than four decades, as revealed in the elucidative monographs of Lekhnitskii (1977) and Elishakoff (2005). However, numerous exquisitely written studies on the fabrication, fracture mechanics, thermal stress analysis, stability and vibration of FGM keep deepening our understanding of the distinctive behaviour of these materials (Benatta, Mechab, Tounsi, & Adda Bedia, 2008; Erdogan, 1995; Jin & Batra, 1996; Liu et al., 2007; Omori, Kakita, Okubo, & Hirai, 1999; Ravichandran, 1995; Reddy & Chin, 1998; Shen, 2002; Şimşek, 2009; Subra Suresh, 1998; Teixeira, Andritschky, & Stöver, 1999; Zhou & Wang, 2006). Among the recent contribution to the literature on the dynamics of functionally graded (FG) structures is the study by Ying, Lü, and Chen (2008), where the state-space method is employed to furnish the exact solutions for free vibration of FG beams resting on a Winkler–Pasternak elastic foundation. The forced vibration of a laminated FG beam under thermally induced initial stresses is studied by Xiang and Yang (2008). Liu and Shu (2014) presented the effects of delamination (its length and location) on the vibration of exponential FG beams. The size-dependent dynamic behaviour of FG beams has also been reported in Refs. (Asghari, Ahmadian, Kahrobaiyan, & Rahaeifard, 2010; Reddy, 2011; Şimşek et al., 2012). With respect to the size-dependent behaviour of micro-scale structural elements, it appears, from the available literature, that research investigations have been focused on FG one-dimensional structures. This is reflected in the study by Akgöz and Civalek (2013a, 2013b) among others, where the size-dependent dynamics of FG micro-scale beams and bars are studied. Contrarily, very few studies are available on the size-dependent dynamics of FG two-dimensional structures like plate and panels as reported by Thai and Kim (2013) and Arani, Kolahchi, Barzoki, Mozdianfard, and Farahani (2012).

The aim of the current study is to examine the coupled extensional-flexural dynamics of a system of connected FG micro-scale panels. As a part of an ongoing design of a micro-scale vibration isolator derived from hybrid materials, the system being investigated in this study deals with the extension of the MCST and the mechanics of FGMs to the analysis of the vibratory response of two inhomogeneous FG micro-panels connected by a series of fixed-fixed bars. The rest of this paper proceeds as follows. In Section 2, the homogenisation scheme for the constituent material is presented. Section 3 details the derivation of the elastodynamics governing equation of the FG micro-scale panels within the framework of the size-dependent theory of MCST. The semi-analytical solution procedure, based on the Navier's method of solution, is presented in Section 4. Discussion of the numerical results is given in Section 5. Basic conclusion that can be deduced from the analyses is given in Section 6.

2. Homogenisation scheme for the constituent material

The effective material properties of the FG micro-panel with a uniform thickness h are evaluated using the rule of mixture (Reddy & Chin, 1998). In what follows, the parameter V denotes the volume fraction, while subscripts m and c denote polymeric matrix phase and the ceramic phase, respectively. It is important to ensure that the total volume fraction of the homogenised material is unity, which is necessary for the homogenisation of the material properties of a FG structure, (Chakraborty, Gopalakrishnan, & Reddy, 2003). Hence:

$$V_m + V_c = 1 \quad (1)$$

In view of the stipulated procedures of the rule of mixture (Reddy & Chin, 1998), the volume fractions of the polymeric and ceramic phases are related to the power-law index n and the thickness of the micro-panel as:

$$V_c(z) = \left(\frac{2z+h}{2h}\right)^n; \quad V_m(z) = 1 - \left(\frac{2z+h}{2h}\right)^n \quad (2a, b)$$

Now, if an effective material property is represented by, say f_e , then it is necessary to relate f_e to the volume fraction of the entire structure in the form:

$$f_e(z) = (f_e)_m V_m + (f_e)_c V_c = [(f_e)_c - (f_e)_m] \left(\frac{2z+h}{2h}\right)^n + (f_e)_m \quad (3)$$

With Equation (3), any actual effective material properties of the FG micro-panel can be derived. Figure 1 depicts the variation of the effective Young's modulus (normalised by the Young's modulus of the polymeric phase) with respect to the micro-panel's thickness for different values of the gradient index n .

3. Theoretical formulation

3.1. Overview of the MCST

In Figure 2, the system of two FG micro-scale panels connected by a two-dimensional array of fixed-fixed bars is shown. In what follows, the governing equation of each

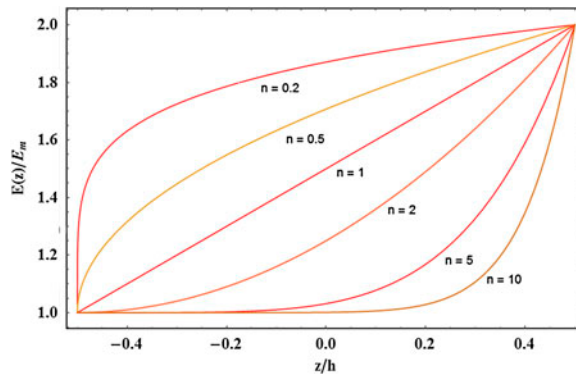


Figure 1. The variation of the normalised Young's modulus as a function of the thickness for different values of the power-law index n .

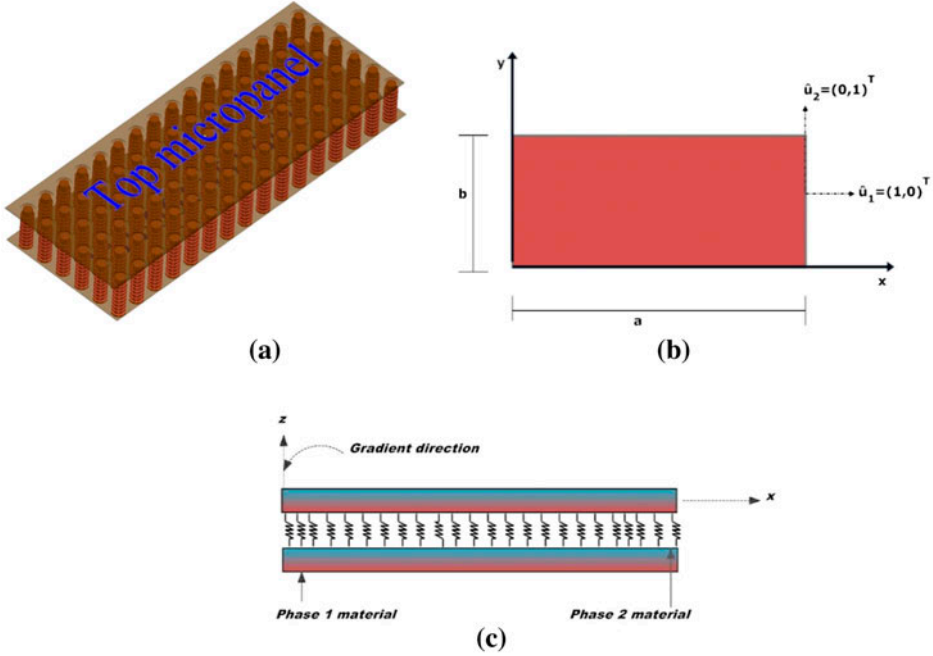


Figure 2. (a) A three-dimensional view of the coupled system; (b) the top view with the adopted coordinate; and (c) side view of the panel showing the gradation direction.

micro-panel is derived from the duo of the MCST and the extended Hamilton's principle. The geometric dimension of each micro-panel is in the form of length (a), width (b) and two plane faces separated by the thickness h . Under the action of a system of bending forces, the following displacement trial field can be assumed:

$$\mathbf{u} = u_1 \mathbf{e}_1 + u_2 \mathbf{e}_2 + u_3 \mathbf{e}_3 \quad (4)$$

where $\mathbf{e}_i (i = 1, 2, 3)$ are unit vectors and u_1 , u_2 and u_3 are components of the displacement vector of an arbitrary material point of the micro-panel in the x , y and z direction of the adopted right-handed rectangular Cartesian coordinate system. Without loss of generality, it has been assumed that each micro-panel possesses a neutral plane, which falls on the mid-surface of the panel. Thus, the small-deflection theory of thin plates, which is predicated on the well-known Kirchhoff's postulates (Szilard, 2004), is adopted and each of the components of the displacement field can be expressed as:

$$u_1(x, y, z, t) = u(x, y, t) - z \frac{\partial w(x, y, t)}{\partial x} \quad (5a)$$

$$u_2(x, y, z, t) = v(x, y, t) - z \frac{\partial w(x, y, t)}{\partial y} \quad (5b)$$

$$u_3(x, y, z, t) = w(x, y, t) \quad (5c)$$

The above displacement trial field, which relies on the displacement u , v and w of the middle surface in the x , y and z directions, is helpful in the mapping of the stress fields created by a set of external system of forces to the instantaneous local deformation of the structure through the requisite higher order constitutive rules. Next, if one assumes the micro-panel to be a macroscopically isotropic linear elastic body occupying a volume \mathcal{V} , then based on the theoretical framework of the MCST, the total strain energy (Π_s) generated by the deformation of this micro-scale panel could be divided into two parts. One part arises from the strain energy contribution of the Cauchy stress tensor (Π_{cs}) and the other part corresponds to the strain energy contribution of the modified couple stress tensor (Π_{ms}). This then leads to the total strain energy to be characterised by a quartet of tensors related as (Reddy, 2011; Yang et al., 2002):

$$\Pi_s = \Pi_{cs} + \Pi_{ms} = \frac{1}{2} \int_{\mathcal{V}} (\boldsymbol{\sigma} : \boldsymbol{\varepsilon}) d\mathcal{V} + \frac{1}{2} \int_{\mathcal{V}} (\mathbf{m} : \boldsymbol{\chi}) d\mathcal{V} \quad (6)$$

Ideally, for each micro-panel, the volume \mathcal{V} is taken to be an open set in \mathbb{R}^3 with a well-behaved surface boundary (see Figure 2(b) for the unit normal to the boundaries' of a micro-panel). The terms $\boldsymbol{\varepsilon}$, and $\boldsymbol{\sigma}$ (in Equation (6)) are the dilatation strain and the Cauchy stress tensors, respectively. Additionally, the tensors \mathbf{m} and $\boldsymbol{\chi}$ refer to the deviatoric component of the couple stress and the symmetric curvature tensor, respectively.

The deformation of a material point in the cross-section of a single micro-panel is described through the displacement field (\mathbf{u}) and a rotation vector ($\boldsymbol{\theta}$) associated with the point. With the help of the displacement field \mathbf{u} and the rotation vector $\boldsymbol{\theta}$, the local instantaneous configuration of the material point can be inferred from the tensors $\boldsymbol{\varepsilon}$ and $\boldsymbol{\chi}$. In general, these tensors satisfy the following geometric relations (Yang et al., 2002):

$$\boldsymbol{\varepsilon} = \frac{1}{2} [\nabla \mathbf{u} + (\nabla \mathbf{u})^T]; \quad \boldsymbol{\chi} = \frac{1}{2} [\nabla \boldsymbol{\theta} + (\nabla \boldsymbol{\theta})^T]; \quad \boldsymbol{\theta} = \frac{1}{2} \text{curl } \mathbf{u} \quad (7a, b, c)$$

where the operator ∇ is the gradient notation. Furthermore, the Cauchy stress field ($\boldsymbol{\sigma}$) and the couple stress field (\mathbf{m}) are related to the displacement field through the higher order constitutive rules as:

$$\boldsymbol{\sigma} = \lambda \text{tr}(\boldsymbol{\varepsilon}) \mathbf{I} + 2G\boldsymbol{\varepsilon}; \quad \mathbf{m} = 2\zeta^2 G\boldsymbol{\chi} \quad (8a, b)$$

In Equation (8), the stress field is mapped to the displacement through the well-known material parameters λ (the bulk modulus) and G (the shear modulus), respectively. Similarly, the higher order stress field is mapped to the displacement through an additional material constant in the form of ζ . This new material constant is related to the material length scale parameter. Using Equation (7), one obtains the non-zero components of the strain tensor, based on the displacement components defined in Equation (5), as:

$$\varepsilon_{xx} = \frac{\partial u}{\partial x} - z\varphi_x = \frac{\partial u}{\partial x} - z \frac{\partial^2 w}{\partial x^2}; \quad \varepsilon_{yy} = \frac{\partial v}{\partial y} - z\varphi_y = \frac{\partial v}{\partial y} - z \frac{\partial^2 w}{\partial y^2} \quad (9a, b)$$

$$\varepsilon_{xy} = \varepsilon_{yx} = \left[\frac{1}{2} \frac{\partial u}{\partial y} + \frac{1}{2} \frac{\partial v}{\partial x} - z \frac{\partial^2 w}{\partial y \partial x} \right] \quad (10)$$

The first term on the right-hand sides of Equations (9(a) and (b)) denotes the strain components in the mid-surface of the micro-panel due to its stretching, while the second term relates to the flexural motion of the FG micro-panel. However, in

Equation (10), the first two terms on the right-hand side relates to the strain components due to stretching, while the third term relates to the transverse motion. The components of the rotation vector, from Equation (7(c)), are obtained as:

$$\theta_x = \frac{\partial w}{\partial x}; \quad \theta_y = -\frac{\partial w}{\partial y}; \quad \theta_z = \frac{1}{2} \left[-\frac{\partial u}{\partial y} + \frac{\partial v}{\partial x} \right] \quad (11)$$

The symmetric curvature tensor (χ_{ij}) has nine components just like the strain tensor. By using the expressions for the rotation vector in Equation (18), bearing in mind Equation (11), one obtains the components of the symmetric curvature tensor as:

$$\chi_{xx} = \frac{\partial^2 w}{\partial y \partial x}; \quad \chi_{yy} = -\frac{\partial^2 w}{\partial y \partial x}; \quad \chi_{zz} = 0 \quad (12a, b, c)$$

$$\chi_{xy} = \frac{1}{2} \left[-\frac{\partial^2 w}{\partial x^2} + \frac{\partial^2 w}{\partial y^2} \right]; \quad \chi_{zy} = \chi_{yz} = \frac{1}{4} \left[-\frac{\partial^2 u}{\partial y \partial x} + \frac{\partial^2 v}{\partial x^2} \right]; \quad \chi_{zx} = \chi_{xz} = \frac{1}{4} \left[-\frac{\partial^2 u}{\partial y^2} + \frac{\partial^2 v}{\partial y \partial x} \right] \quad (13a, b, c)$$

Since the stress tensors represent a mapping from the vector space of surface deformations to the vector space of forces, the stress–strain relationships are used to obtain the stress–curvature relationships as (see the Appendix 1 for detail).

3.2. Elastodynamics governing equations

In line with the requirement of the Hamilton's principles, the first variation of the inhomogeneous, microstructure-dependent strain energy is now written as:

$$\begin{aligned} \delta \Pi_S = & \frac{1}{2} \delta \iint \int_{-h/2}^{h/2} \left[\frac{E(z)}{(1-\nu^2)} \varepsilon_{xx}^2 + \frac{E(z)}{(1-\nu^2)} \varepsilon_{yy}^2 + \frac{2\nu E(z)}{(1-\nu^2)} \varepsilon_{xy} \varepsilon_{yx} + \frac{E(z)}{(1+\nu)} \varepsilon_{yx}^2 \right] dx dy dz \\ & + \frac{1}{2} \delta \iint \int_{-h/2}^{h/2} G(z) \left[\zeta^2 \mu (2\chi_{xx})^2 + \zeta^2 \mu (2\chi_{yy})^2 + \zeta^2 \mu (2\chi_{xy})^2 + \zeta^2 \mu (2\chi_{yz})^2 + \zeta^2 \mu (2\chi_{xz})^2 \right] dx dy dz \end{aligned} \quad (14)$$

The underlined terms in Equation (14) are due to the couple stress effect. In a similar spirit, the components of the displacement field defined in Equation (5) are used to establish the first variation of the kinetic energy of an element of the FG micro-panel, with the rotary inertia included, as (Reddy, 2002; Szilard, 2004):

$$\delta \Pi_T = \frac{1}{2} \delta \int_A \int_{-h/2}^{h/2} \rho(z) \left[\left(\frac{\partial u_1}{\partial t} \right)^2 + \left(\frac{\partial u_2}{\partial t} \right)^2 + \left(\frac{\partial u_3}{\partial t} \right)^2 \right] dz dA \quad (15)$$

where $\rho(z)$ is the variable mass density of the micro-panel. The first variation of the virtual work done due to external loads is:

$$\delta \Pi_B = - \int_R (f_i \delta u_i + c_i \delta \theta_i) dA - \int_{\partial R} (t_i \delta u_i + s_i \delta \theta_i) ds \quad (16)$$

where f_i , c_i , t_i and s_i are the body force, the body couple, the traction and the surface couple, respectively. As expected, the body force and the body couple are integrated over the area R which contains the mid-surface of the micro-panel, while the traction

and surface couple are integrated over the boundary ∂R . Within the time interval t_1 and t_2 describing the trajectory of the motion of a conservative system, the mathematical statement of the Hamilton's principle states that (Reddy, 2002):

$$\delta \int_{t_1}^{t_2} (\Pi_T - \Pi_S + \Pi_B) dt = 0 \quad (17)$$

Thus, after substituting Equations (14)–(16) into Equation (17), and integrating each term of the integrals in Equation (17) by parts, one employs the fundamental lemma of variational to obtain the size-dependent, governing equations of a single micro-panel as:

$$\begin{aligned} A_1 \frac{\partial^2 u}{\partial t^2} + A_2 \frac{\partial^2 u}{\partial y^2} - A_3 \frac{\partial^4 u}{\partial y^4} + A_4 \frac{\partial^3 w}{\partial x \partial t^2} - A_5 \frac{\partial^2 v}{\partial x \partial y} + A_6 \frac{\partial^3 w}{\partial x \partial y^2} + A_7 \frac{\partial^4 v}{\partial x \partial y^3} \\ - A_8 \frac{\partial^2 u}{\partial x^2} - A_9 \frac{\partial^4 u}{\partial x^2 \partial y^2} + A_{10} \frac{\partial^3 w}{\partial x^3} + A_{11} \frac{\partial^4 v}{\partial x^3 \partial y} = 0 \end{aligned} \quad (18)$$

$$\begin{aligned} B_1 \frac{\partial^2 v}{\partial t^2} + B_2 \frac{\partial^3 w}{\partial y \partial t^2} - B_3 \frac{\partial^2 v}{\partial y^2} + B_4 \frac{\partial^3 w}{\partial y^3} - B_5 \frac{\partial^2 u}{\partial x \partial y} + B_6 \frac{\partial^4 u}{\partial x \partial y^3} + B_7 \frac{\partial^2 v}{\partial x^2} + B_8 \frac{\partial^3 w}{\partial x^2 \partial y} \\ - B_9 \frac{\partial^4 v}{\partial x^2 \partial y^2} + B_{10} \frac{\partial^4 u}{\partial x^3 \partial y} - B_{11} \frac{\partial^4 v}{\partial x^4} = 0 \end{aligned} \quad (19)$$

$$\begin{aligned} C_1 \frac{\partial^2 w}{\partial t^2} - C_2 \frac{\partial^3 v}{\partial y \partial t^2} + C_3 \frac{\partial^4 w}{\partial y^2 \partial t^2} - C_4 \frac{\partial^3 v}{\partial y^3} - C_5 \frac{\partial^3 u}{\partial x \partial t^2} - C_6 \frac{\partial^3 u}{\partial x \partial y^2} + C_7 \frac{\partial^4 w}{\partial x^2 \partial t^2} \\ - C_8 \frac{\partial^3 v}{\partial y \partial x^2} - C_9 \frac{\partial^3 u}{\partial x^3} + C_{10} \frac{\partial^4 w}{\partial y^4} + C_{11} \frac{\partial^4 w}{\partial x^2 \partial y^2} + C_{12} \frac{\partial^4 w}{\partial x^4} = 0 \end{aligned} \quad (20)$$

The coefficient $A_1 - A_{10}$, $B_1 - B_{10}$ and $C_1 - C_{12}$ in Equations (18)–(20) are defined in Appendix 1, for brevity sake. There are two limiting cases of interest that can be derived from the above set of governing equations. The first is the governing equations of a FG panel with no microstructural material constant, and these are obtained by setting $\zeta = 0$ in the above expressions to arrive at:

$$\begin{aligned} \frac{h\rho_m(n + \rho_r)}{1 + n} \frac{\partial^2 u}{\partial t^2} + \frac{hE_m(n + E_r)}{2(1 + n)(1 + v)} \frac{\partial^2 u}{\partial y^2} + \frac{h^2 n \rho_m(-1 + \rho_r)}{2(1 + n)(2 + n)} \frac{\partial^3 w}{\partial x \partial t^2} \\ - \frac{hE_m(n + E_r)}{2(1 + n)(-1 + v)} \frac{\partial^2 v}{\partial x \partial y} + \frac{h^2 n E_m(-1 + E_r)}{2(1 + n)(2 + n)(-1 + v)(1 + v)} \frac{\partial^3 w}{\partial x \partial y^2} \\ - \frac{hE_m(n + E_r)}{(1 + n)(-1 + v)(1 + v)} \frac{\partial^2 u}{\partial x^2} + \frac{h^2 n E_m(-1 + E_r)}{2(1 + n)(2 + n)(-1 + v)(1 + v)} \frac{\partial^3 w}{\partial x^3} = 0 \end{aligned} \quad (21)$$

$$\begin{aligned} - \frac{h\rho_m(n + \rho_r)}{1 + n} \frac{\partial^2 v}{\partial t^2} + \frac{h^2 n \rho_m(-1 + \rho_r)}{2(1 + n)(2 + n)} \frac{\partial^3 w}{\partial y \partial t^2} - \frac{hE_m(n + E_r)}{(1 + n)(-1 + v)(1 + v)} \frac{\partial^2 v}{\partial y^2} \\ + \frac{h^2 n E_m(-1 + E_r)}{2(1 + n)(2 + n)(-1 + v)(1 + v)} \frac{\partial^3 w}{\partial y^3} - \frac{hE_m(n + E_r)}{2(1 + n)(-1 + v)} \frac{\partial^2 u}{\partial x \partial y} \\ + \frac{hE_m(n + E_r)}{2(1 + n)(1 + v)} \frac{\partial^2 v}{\partial x^2} + \frac{h^2 n E_m(-1 + E_r)}{2(1 + n)(2 + n)(-1 + v)(1 + v)} \frac{\partial^3 w}{\partial x^2 \partial y} = 0 \end{aligned} \quad (22)$$

$$\begin{aligned}
& -\frac{h\rho_m(n+\rho_r)}{1+n}\frac{\partial^2 w}{\partial t^2} - \frac{h^2 n\rho_m(-1+\rho_r)}{2(1+n)(2+n)}\frac{\partial^3 v}{\partial y\partial t^2} + \frac{h^3\rho_m(n^3+6\rho_r+3n^2(1+\rho_r)+n(8+3\rho_r))}{12(1+n)(2+n)(3+n)}\frac{\partial^4 w}{\partial y^2\partial t^2} \\
& - \frac{h^2 nEe_m(-1+Ee_r)}{2(1+n)(2+n)(-1+v)(1+v)}\frac{\partial^3 v}{\partial y^3} - \frac{h^2 n\rho_m(-1+\rho_r)}{2(1+n)(2+n)}\frac{\partial^3 u}{\partial x\partial t^2} \\
& - \frac{h^2 nEe_m(-1+Ee_r)}{2(1+n)(2+n)(-1+v)(1+v)}\frac{\partial^3 u}{\partial x\partial y^2} \\
& + \frac{h^3\rho_m(n^3+6\rho_r+3n^2(1+\rho_r)+n(8+3\rho_r))}{12(1+n)(2+n)(3+n)}\frac{\partial^4 w}{\partial x^2\partial t^2} \\
& - \frac{h^2 nEe_m(-1+Ee_r)}{2(1+n)(2+n)(-1+v)(1+v)}\frac{\partial^3 v}{\partial y\partial x^2} - \frac{h^2 nEe_m(-1+Ee_r)}{2(1+n)(2+n)(-1+v)(1+v)}\frac{\partial^3 u}{\partial x^3} \\
& + Q_1\frac{\partial^4 w}{\partial y^4} + Q_2\frac{\partial^4 w}{\partial x^2\partial y^2} + Q_3\frac{\partial^4 w}{\partial x^4} = 0
\end{aligned} \tag{23}$$

where $Q_j(j = 1, 2, 3)$ are defined in Appendix 1. The second limiting case is the governing equation of a micro-scale panel made of a homogeneous polymeric material with no functional gradation. This set of equations is obtained by setting $n = 0$, $E_r = 1$, $G_r = 1$ and $\rho_r = 1$ in Equations (18)–(20) to retrieve:

$$\begin{aligned}
& -\rho_m h\frac{\partial^2 u}{\partial t^2} + E_m h\left[\frac{1}{2(1+v)}\frac{\partial^2 u}{\partial y^2} + \frac{1}{2(1-v)}\frac{\partial^2 v}{\partial y\partial x} + \frac{1}{1-v^2}\frac{\partial^2 u}{\partial x^2}\right] \\
& + \frac{E_m h\zeta^2}{8(1+v)}\left[\frac{\partial^4 v}{\partial y^3\partial x} - \frac{\partial^4 u}{\partial y^4} - \frac{\partial^4 u}{\partial x^2\partial y^2} + \frac{\partial^4 v}{\partial x^3\partial y}\right] = 0
\end{aligned} \tag{24}$$

$$\begin{aligned}
& -\rho_m h\frac{\partial^2 v}{\partial t^2} + E_m h\left[\frac{1}{1-v^2}\frac{\partial^2 v}{\partial y^2} + \frac{1}{2(1-v)}\frac{\partial^2 u}{\partial y\partial x} + \frac{1}{2(1+v)}\frac{\partial^2 v}{\partial x^2}\right] \\
& + \frac{E_m h\zeta^2}{8(1+v)}\left[\frac{\partial^4 u}{\partial y^3\partial x} - \frac{\partial^4 v}{\partial x^2\partial y^2} + \frac{\partial^4 u}{\partial x^3\partial y} - \frac{\partial^4 v}{\partial x^4}\right] = 0
\end{aligned} \tag{25}$$

$$\begin{aligned}
& -\rho_m h\frac{\partial^2 w}{\partial t^2} + \rho_m I\left[\frac{\partial^4 w}{\partial t^2\partial y^2} + \frac{\partial^4 w}{\partial t^2\partial x^2}\right] - \frac{E_m h^3}{12(1-v^2)}\left[\frac{\partial^4 w}{\partial y^4} + 2\frac{\partial^4 w}{\partial x^2\partial y^2} + \frac{\partial^4 w}{\partial x^4}\right] \\
& - \frac{E_m h\zeta^2}{2(1+v)}\left[\frac{\partial^4 w}{\partial y^4} + 2\frac{\partial^4 w}{\partial x^2\partial y^2} + \frac{\partial^4 w}{\partial x^4}\right] = 0
\end{aligned} \tag{26}$$

From the physical point of view, Equations (18)–(20) represent the vibration behaviour of a single FG micro-scale panel. Besides, from the nature of Equations (18)–(20), it would be noticed that the three field variables, which include two extensional deformations (u and v) and one flexural deformation (w), exist in each of Equations (18)–(20). The existence of each variable in the three governing equations of motions of the system reveals the coupling of the extensional-flexural vibration modes for the FG micro-scale panel. Contrarily, only the extensional deformation field variables are coupled in the case of the non-FG micro-scale (as reflected in Equations (24)–(26)).

In order to deal with the acceptable magnitude of the stiffness for the elastic connectors, three basic assumptions are made. First, it is assumed that the elastic connectors are made of similar materials. Second, the elastic connectors suffer negligible distortion of their positions with respect to their initial contact positions with the surface of each FG micro-panel. Third, no structural anisotropy is introduced by the elastic connectors. Besides, it is also assumed that the two micro-panels are made of the same

material, length, width and density. Given these assumptions, the rigidities of the elastic connectors is replaced by a distributed continuous foundation of the Winkler's type with an effective stiffness denoted by K_t . The effective stiffness (K_t) is then estimated to be the averaged stiffness of the connectors between the micro-panels. As earlier noted, the coupled system being investigated is to be employed in a vibration isolation pad for electronic systems. In this wise, the elastic connectors would be designed to have resistance to stretching and compression. With this premise, each elastic connector is idealised as a fixed-fixed bar, with an estimated equivalent stiffness k_r . The contribution of the bars' stiffness is now reflected in the vibration governing equation of the individual micro-panel as:

3.2.1. Upper micro-panel

$$\begin{aligned} A_1 \frac{\partial^2 u_t}{\partial t^2} + A_2 \frac{\partial^2 u_t}{\partial y^2} - A_3 \frac{\partial^4 u_t}{\partial y^4} + A_4 \frac{\partial^3 w_t}{\partial x \partial t^2} - A_5 \frac{\partial^2 v_t}{\partial x \partial y} + A_6 \frac{\partial^3 w_t}{\partial x \partial y^2} + A_7 \frac{\partial^4 v_t}{\partial x \partial y^3} \\ - A_8 \frac{\partial^2 u_t}{\partial x^2} - A_9 \frac{\partial^4 u_t}{\partial x^2 \partial y^2} + A_{10} \frac{\partial^3 w_t}{\partial x^3} + A_{11} \frac{\partial^4 v_t}{\partial x^3 \partial y} = 0 \end{aligned} \quad (27)$$

$$\begin{aligned} -B_1 \frac{\partial^2 v_t}{\partial t^2} + B_2 \frac{\partial^3 w_t}{\partial y \partial t^2} - B_3 \frac{\partial^2 v_t}{\partial y^2} + B_4 \frac{\partial^3 w_t}{\partial y^3} - B_5 \frac{\partial^2 u_t}{\partial x \partial y} + B_6 \frac{\partial^4 u_t}{\partial x \partial y^3} + B_7 \frac{\partial^2 v_t}{\partial x^2} + B_8 \frac{\partial^3 w_t}{\partial x^2 \partial y} \\ - B_9 \frac{\partial^4 v_t}{\partial x^2 \partial y^2} + B_{10} \frac{\partial^4 u_t}{\partial x^3 \partial y} - B_{11} \frac{\partial^4 v_t}{\partial x^4} = 0 \end{aligned} \quad (28)$$

$$\begin{aligned} -C_1 \frac{\partial^2 w_t}{\partial t^2} - C_2 \frac{\partial^3 v_t}{\partial y \partial t^2} + C_3 \frac{\partial^4 w_t}{\partial y^2 \partial t^2} - C_4 \frac{\partial^3 v_t}{\partial y^3} - C_5 \frac{\partial^3 u_t}{\partial x \partial t^2} - C_6 \frac{\partial^3 u_t}{\partial x \partial y^2} + C_7 \frac{\partial^4 w_t}{\partial x^2 \partial t^2} \\ - C_8 \frac{\partial^3 v_t}{\partial y \partial x^2} - C_9 \frac{\partial^3 u_t}{\partial x^3} + C_{10} \frac{\partial^4 w_t}{\partial y^4} + C_{11} \frac{\partial^4 w_t}{\partial x^2 \partial y^2} + C_{12} \frac{\partial^4 w_t}{\partial x^4} + K_t(w_t - w_b) = 0 \end{aligned} \quad (29)$$

3.2.2. Lower micro-panel

$$\begin{aligned} A_1 \frac{\partial^2 u_b}{\partial t^2} + A_2 \frac{\partial^2 u_b}{\partial y^2} - A_3 \frac{\partial^4 u_b}{\partial y^4} + A_4 \frac{\partial^3 w_b}{\partial x \partial t^2} - A_5 \frac{\partial^2 v_b}{\partial x \partial y} + A_6 \frac{\partial^3 w_b}{\partial x \partial y^2} + A_7 \frac{\partial^4 v_b}{\partial x \partial y^3} - A_8 \frac{\partial^2 u_b}{\partial x^2} \\ - A_9 \frac{\partial^4 u_b}{\partial x^2 \partial y^2} + A_{10} \frac{\partial^3 w_b}{\partial x^3} + A_{11} \frac{\partial^4 v_b}{\partial x^3 \partial y} = 0 \end{aligned} \quad (30)$$

$$\begin{aligned} -B_1 \frac{\partial^2 v_b}{\partial t^2} + B_2 \frac{\partial^3 w_b}{\partial y \partial t^2} - B_3 \frac{\partial^2 v_b}{\partial y^2} + B_4 \frac{\partial^3 w_b}{\partial y^3} - B_5 \frac{\partial^2 u_b}{\partial x \partial y} + B_6 \frac{\partial^4 u_b}{\partial x \partial y^3} + B_7 \frac{\partial^2 v_b}{\partial x^2} + B_8 \frac{\partial^3 w_b}{\partial x^2 \partial y} \\ - B_9 \frac{\partial^4 v_b}{\partial x^2 \partial y^2} + B_{10} \frac{\partial^4 u_b}{\partial x^3 \partial y} - B_{11} \frac{\partial^4 v_b}{\partial x^4} = 0 \end{aligned} \quad (31)$$

$$\begin{aligned}
& -C_1 \frac{\partial^2 w_b}{\partial t^2} - C_2 \frac{\partial^3 v_b}{\partial y \partial t^2} + C_3 \frac{\partial^4 w_b}{\partial y^2 \partial t^2} - C_4 \frac{\partial^3 v_b}{\partial y^3} - C_5 \frac{\partial^3 u_b}{\partial x \partial t^2} - C_6 \frac{\partial^3 u_b}{\partial x \partial y^2} + C_7 \frac{\partial^4 w_b}{\partial x^2 \partial t^2} \\
& - C_8 \frac{\partial^3 v_b}{\partial y \partial x^2} - C_9 \frac{\partial^3 u_b}{\partial x^3} + C_{10} \frac{\partial^4 w_b}{\partial y^4} + C_{11} \frac{\partial^4 w_b}{\partial x^2 \partial y^2} + C_{12} \frac{\partial^4 w_b}{\partial x^4} - K_t(w_t - w_b) = 0
\end{aligned} \tag{32}$$

In Equations (27)–(32), u_t , v_t and w_t are the field variables for the top FG micro-panel, while u_b , v_b and w_b are the field variables for the base FG micro-panel. The problem above can be made a bit tractable, if the displacement transverse field variables describing the behaviour of each FG micro-panel are homogenised through the method of sequential subtraction (as done, for instance, in Murmu (Murmu & Adhikari, 2011)) to get:

$$\begin{aligned}
& A_1 \frac{\partial^2 u_h}{\partial t^2} + A_2 \frac{\partial^2 u_h}{\partial y^2} - A_3 \frac{\partial^4 u_h}{\partial y^4} + A_4 \frac{\partial^3 w_h}{\partial x \partial t^2} - A_5 \frac{\partial^2 v_h}{\partial x \partial y} + A_6 \frac{\partial^3 w_h}{\partial x \partial y^2} + A_7 \frac{\partial^4 v_h}{\partial x \partial y^3} - A_8 \frac{\partial^2 u_h}{\partial x^2} \\
& - A_9 \frac{\partial^4 u_h}{\partial x^2 \partial y^2} + A_{10} \frac{\partial^3 w_h}{\partial x^3} + A_{11} \frac{\partial^4 v_h}{\partial x^3 \partial y} = 0
\end{aligned} \tag{33}$$

$$\begin{aligned}
& -B_1 \frac{\partial^2 v_h}{\partial t^2} + B_2 \frac{\partial^3 w_h}{\partial y \partial t^2} - B_3 \frac{\partial^2 v_h}{\partial y^2} + B_4 \frac{\partial^3 w_h}{\partial y^3} - B_5 \frac{\partial^2 u_h}{\partial x \partial y} + B_6 \frac{\partial^4 u_h}{\partial x \partial y^3} + B_7 \frac{\partial^2 v_h}{\partial x^2} + B_8 \frac{\partial^3 w_h}{\partial x^2 \partial y} \\
& - B_9 \frac{\partial^4 v_h}{\partial x^2 \partial y^2} + B_{10} \frac{\partial^4 u_h}{\partial x^3 \partial y} - B_{11} \frac{\partial^4 v_h}{\partial x^4} = 0
\end{aligned} \tag{34}$$

$$\begin{aligned}
& -C_1 \frac{\partial^2 w_h}{\partial t^2} - C_2 \frac{\partial^3 v_h}{\partial y \partial t^2} + C_3 \frac{\partial^4 w_h}{\partial y^2 \partial t^2} - C_4 \frac{\partial^3 v_h}{\partial y^3} - C_5 \frac{\partial^3 u_t}{\partial x \partial t^2} - C_6 \frac{\partial^3 u_h}{\partial x \partial y^2} + C_7 \frac{\partial^4 w_h}{\partial x^2 \partial t^2} \\
& - C_8 \frac{\partial^3 v_h}{\partial y \partial x^2} - C_9 \frac{\partial^3 u_h}{\partial x^3} + C_{10} \frac{\partial^4 w_h}{\partial y^4} + C_{11} \frac{\partial^4 w_h}{\partial x^2 \partial y^2} + C_{12} \frac{\partial^4 w_h}{\partial x^4} + 2K(w_h) = 0
\end{aligned} \tag{35}$$

where the following change of variable has been employed:

$$u_h = u_t; \quad v_h = v_t; \quad w_h = w_t - w_b \tag{36}$$

With Equations (33)–(35), the vibration characteristics of the system is examined under an idealised boundary conditions in the form of simple supports on the four edges (SSSS) of the coupled micro-panels as shown in Figure 3.

In order to specify the expressions for the stipulated boundary conditions, the following stress resultants are defined:

$$\left\{ \begin{array}{c} C_{xx} \\ C_{xy} \\ C_{xz} \\ C_{yy} \\ C_{yz} \end{array} \right\} = \int_{-h/2}^{h/2} \left\{ \begin{array}{c} m_{xx} \\ m_{xy} \\ m_{xz} \\ m_{yy} \\ m_{yz} \end{array} \right\} dz \tag{37}$$

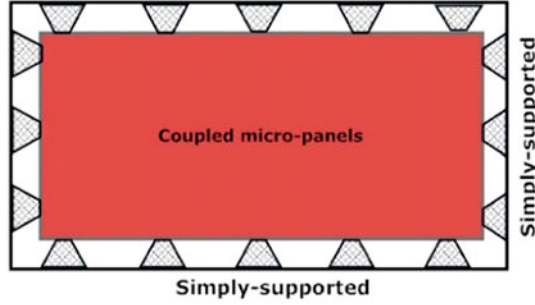


Figure 3. Schematics of the top-view of the FG micro-panel with simple supports on the four edges.

$$\begin{Bmatrix} N_{xx} \\ N_{xy} \\ N_{yy} \end{Bmatrix} = \int_{-h/2}^{h/2} \begin{Bmatrix} \sigma_{xx} \\ \sigma_{xy} \\ \sigma_{yy} \end{Bmatrix} dz \quad (38a)$$

$$\begin{Bmatrix} M_{xx} \\ M_{xy} \\ M_{yy} \end{Bmatrix} = \int_{-h/2}^{h/2} \begin{Bmatrix} \sigma_{xx} \\ \sigma_{xy} \\ \sigma_{yy} \end{Bmatrix} z dz \quad (38b)$$

where C_{xx} , C_{xy} , C_{xz} , C_{yy} and C_{yz} are the couple moments that needs to be mapped to the displacement field through Equation (8(b)). Also, M_{xx} , M_{xy} and M_{yy} are the moments (related to the Cauchy stress) that are mapped to the displacement field through Equation (8(a)). Under the SSSS boundary condition, the following constraints are imposed around the periphery of the coupled FG micro-panels:

$$w_h(0, y, t) = w_t(0, y, t) - w_b(0, y, t) = 0 \quad (39)$$

$$w_h(a, 0, t) = w_t(a, 0, t) - w_b(a, 0, t) = 0 \quad (40)$$

$$w_h(x, 0, t) = w_t(x, 0, t) - w_b(x, 0, t) = 0 \quad (41)$$

$$w_h(x, b, t) = w_t(x, b, t) - w_b(x, b, t) = 0 \quad (42)$$

$$M_{xch}(0, y, t) + C_{xya}(0, y, t) + N_{xx}(0, y, t) = 0 \quad (43)$$

$$M_{xch}(a, y, t) + C_{xya}(a, y, t) + N_{xx}(a, y, t) = 0 \quad (44)$$

$$-M_{yyh}(x, 0, t) + C_{xya}(x, 0, t) + N_{yy}(x, 0, t) = 0 \quad (45)$$

$$-M_{yyh}(x, b, t) + C_{xya}(x, b, t) + N_{yy}(x, b, t) = 0 \quad (46)$$

4. Analytical solution

The Navier method of solution is adopted to evaluate the dynamic response of the coupled system. In this wise, the field variables in the governing equation of the coupled system of micro-panels are transformed into the following double series:

$$u(x, y, t) = \sum_{p=1}^{\infty} \sum_{q=1}^{\infty} D_{pq} \cos\left(\frac{p\pi x}{a}\right) \sin\left(\frac{q\pi y}{b}\right) e^{i\omega t} \quad (47)$$

$$v(x, y, t) = \sum_{p=1}^{\infty} \sum_{q=1}^{\infty} F_{pq} \sin\left(\frac{p\pi x}{a}\right) \cos\left(\frac{q\pi y}{b}\right) e^{i\omega t} \quad (48)$$

$$w(x, y, t) = \sum_{p=1}^{\infty} \sum_{q=1}^{\infty} H_{pq} \sin\left(\frac{p\pi x}{a}\right) \sin\left(\frac{q\pi y}{b}\right) e^{i\omega t} \quad (49)$$

where p and q are the nodal lines in the x and y directions, respectively. Also, D_{pq} , F_{pq} and H_{pq} represent the amplitude of the two extensional and the transverse vibration modes, respectively. The dimensionality of the governing equation is reduced by introducing the following non-dimensional parameters:

$$\xi = x/a; \quad \eta = y/b; \quad \phi = a/b \quad (50)$$

$$\gamma = \zeta/h; \quad \beta_{\text{eff}} = Ka^4/D_p; \quad \alpha = a/h; \quad \lambda_{pq} = \omega_{pq}(a^2/h) \sqrt{\rho_m/E_m} \quad (51)$$

where D_p has been introduced in Equations (50)–(51) to denote the flexural rigidity of the micro-panel. That is: $D_p = E_p h^3/12(1 - \nu^2)$. Besides, in the above expressions, the parameter λ_{pq} represents the non-dimensional natural frequency.

By substituting Equations (47)–(49) into Equations (33)–(35), one obtains the transformed governing equations in the form:

$$\begin{bmatrix} W_{11} & W_{12} & W_{13} \\ W_{21} & W_{22} & W_{23} \\ W_{31} & W_{32} & W_{33} \end{bmatrix} \begin{Bmatrix} D_{pq} \\ F_{pq} \\ H_{pq} \end{Bmatrix} = \begin{Bmatrix} 0 \\ 0 \\ 0 \end{Bmatrix} \quad (52)$$

The coefficients of the characteristics matrix above are detailed in the Appendix 1. Of course, for the natural frequency to be determined, the non-trivial solution of Eq. (74) is sought by making the determinant of the matrix \mathbf{W} to vanish as:

$$|\mathbf{W}| = 0 \quad (53)$$

5. Discussion

In this section, numerical results relating to the sensitivity of the coupled system of FG micro-scale panels is detailed. In the meantime, it is necessary to point out that by looking at the elastically coupled system of the FG micro-panels, two possible mechanistic motions of interests can be achieved by the system. As shown in Figure 4, the transverse motion can be in the form of an asynchronous motion or in the form of a synchronous motion. Principally, under the asynchronous motion of the coupled system, the two FG micro-panels move in different directions, leading to the condition of



Figure 4. Special cases of the transverse motion of the elastically connected micro-panels: (a) asynchronous transverse motion; and (b) synchronous transverse motion.

motion in which the relative displacement does not vanish (i.e. $w_h \neq 0$). However, in the case of a synchronous motion, the motions of the FG micro-panels system are in the same direction, hence $w_h = 0$. These two special cases are shown in Figure 4.

As pointed out in Section 2, when dealing with FG structures, the effective material properties such as density, Young's and shear moduli of the graded structure needs to be determined via the distributions of the volume fraction of the constituent materials. Since FG structures are macroscopically homogeneous, a number of micromechanics models and procedures have been employed in recent years to determine their effective properties. These methods include the Mori–Tanaka homogenisation scheme, the method of the rule of mixture and the self-consistent methods (Chakraborty et al., 2003). The rule of mixture is adopted in the present study, as illustrated in Section 2, to estimate the effective properties of the FG bulk micro-panel.

Furthermore, the traditional design of FG structures involves the use of the top layer (which is often fully ceramic) as a thermal barrier to a metallic structure (the base material). However, recent studies have demonstrated substantial improvement in the performance of FG structures whose base matrix phase is polymer, as demonstrated in Krumova, Klingshirn, Hauptert, and Friedrich (2001). It is in this spirit that in the present study, the top layer acts as a barrier to a polymeric matrix phase. For the matrix phase, therefore, the material properties of an epoxy polymer are employed. This includes Young's modulus (E_m) of 1.44 GPa, mass density (ρ_m) of 1220 kg/m³ and Poisson's ratio (ν) of .38. Additionally, following Ke, Wang, Yang, and Kitipornchai (2012), a conservative value of $\zeta = 17.6 \mu\text{m}$ is used for the material length scale parameter of the epoxy micro-panel. The value for the material length scale parameter used is based on the experimentally determined value (from nano-indentation test of a micron-sized epoxy beams) reported by Lam et al. (2003). Studies have shown that for polymeric structural element, whose underlying macromolecular chains are of finite stiffness, the material length scale (ζ) happens to be directly related to the effective averaged Frank elastic constant (Gao et al., 2013). Moreover, in this study, two different ceramic materials are considered for the functional gradation of the polymer matrix phase. The first is hexagonal boron nitride, and the second is silicon carbide. The mechanical properties of these two ceramic materials are given in Table 1.

5.1. Validation of solution procedure

For a start, we assess the accuracy of the predicted results from the solution procedure, through an initial validation study that is carried out to establish the natural frequency values of each panel as a single structural entity. From the literature review, it is observed that the non-dimensional numerical values of the natural frequencies of micro-plates are not yet as widely published as compared to those of plates with no

Table 1. The mechanical properties of constituents material (Shackelford & Alexander, 2000; Zhang, He, Liu, Gan, & Shen, 2013).

Material property	Boron nitride	Silicon carbide
ρ (kg m ⁻³)	2270	3100
E (GPa)	34	427
ν	.19	.17

micro-scale effect. This is despite the fact that certain aspect of the dynamics studies of a single micro-scale plate have been carried out in some recent studies (Akgöz & Civalek, 2013; Jomehzadeh et al., 2011). Therefore, in this first validation study, a comparative assessment is done with the exact closed-form solution provided in the work of Yin et al. (2010). However, it should be pointed out that the work of Yin et al. (2010) deals with the vibration analysis of a micro-plate with no functional material gradation (that is, a purely homogeneous micro-plate). Thus, this validation requires changes to be made to the derived governing equation through the use of $\beta_{\text{eff}} = 0$, $n = 0$, $E_r = 1$ and $\rho_r = 1$. Table 2 provides the comparison of the non-dimensional frequencies of a micro-plate with simply-supported edges predicted by Yin et al. (2010) and the present study. It is seen from this table that the results of the present study agree well with that of Liu et al. (Yin et al., 2010), for the two vibration modes compared.

Table 3 contains the second validation study. This particular validation study involves a comparison with the work of Baferani, Saidi, and Jomehzadeh (2011), which deals with the vibration of a FG plate based on the classical thin plate theory (that is, with no microstructural effect). This validation study also requires the current model to be reduced. Besides, it involves the elimination of the effects of the elastic connectors and that of the material length scale from the governing equation (that is, $\beta_{\text{eff}} = 0$, $\gamma = 0$). From the results presented in Table 3, a relatively good agreement is observed between the predicted natural frequency of the plate based on the Navier solution method of the current study, and the Levy method of solution employed by Baferani et al. (2011). Besides, the table contains values for three vibration modes (λ_{11} , λ_{12} and λ_{22}) under four values of the gradient index ($n = 0, .5, 1$ and 2) and two values of the

Table 2. Representative frequency parameter of a micro-plate with simply-supported edges.

ϕ	Normalised natural frequency					
	$\gamma = .2$		$\gamma = .5$		$\gamma = .8$	
	Present	Ref. (Yin et al., 2010)	Present	Ref. (Yin et al., 2010)	Present	Ref. (Yin et al., 2010)
(λ_{11})						
$(\beta_{\text{eff}} = 0, \nu = .38)$						
2/3	15.28	15.28	19.81	19.81	26.22	26.22
1.0	21.16	21.16	27.42	27.42	36.29	36.29
1.5	34.38	34.38	44.56	44.56	58.97	58.97
(λ_{12})						
$(\beta_{\text{eff}} = 0, \nu = .38)$						
2/3	29.38	29.38	38.08	38.08	50.46	50.46
1.0	52.89	52.89	68.55	68.55	90.73	90.73
1.5	105.78	105.78	137.11	137.11	181.47	181.47

Table 3. Non-dimensional natural frequencies of a FG plate with simply-supported edges (aluminium functionally graded with aluminium oxide).

Normalised natural frequency $\left(\lambda_{pq} = \omega_{pq}\pi^2(a^2/h)\sqrt{\rho_m/E_m}\right)$ ($\alpha = 100$)		λ_{11}		λ_{12}		λ_{22}	
Gradient index (n)	Aspect ratio (ϕ)	Present study	Baferani et al. (2011)	Present study	Baferani et al. (2011)	Present study	Baferani et al. (2011)
0	1	112.63	115.87	281.58	289.77	449.93	463.47
	.5	70.39	72.39	112.63	—**	281.20	—
.5	1	96.48	98.01	241.22	245.33	385.46	392.44
	.5	60.30	61.33	96.48	—	240.90	—
1	1	88.02	88.31	220.08	221.06	351.69	353.62
	.5	55.01	55.12	88.02	—	219.79	—
2	1	81.35	80.35	203.41	200.88	325.05	321.41
	.5	50.84	50.07	81.359	—	203.13	—

aspect ratio ($\phi = .5$ and 1). It would be observed that all the values obtained from the present solution procedure fall within 3% of those obtained by Baferani et al. (2011). A close examination also reveals that some of the values predicted from the current study differs by less than .5% from those reported by Baferani et al. (2011). For the values of the natural frequency reported in Table 3, the material properties of aluminium and aluminium oxide have been used:

Aluminium: $E = 70$ GPa, $\nu = .3$, $\rho = 2707$ kg/m³;

Aluminium oxide: $E = 320.20$ GPa, $\nu = .26$, $\rho = 3750$ kg/m³;

In addition, the matrix phase is metallic as reflected in the non-dimensional form of the natural frequency written in the form $\lambda_{pq} = \omega_{pq}\pi^2(a^2/h)\sqrt{\rho_m/E_m}$. Figures 5–7 exemplifies the typical pattern of mode shapes λ_{11} , λ_{12} and λ_{22} under three different values of the functional material gradient index. For these plots, the aspect ratio is kept to the value of 1. In Figures 5–7, the mode shape plots are complemented by the contour plot, reflecting the equilibrium positions. It would be noticed (also apparent in Table 2) that higher values of the gradient index lead to a decrease in the natural frequency values.

5.2. Parametric studies

This section consists of the hierarchical qualitative assessment of the influence of the gradient index (n), the span-to-thickness ratio (α), the aspect ratio (ϕ), the density ratio (ρ_r), the elastic modulus ratio (E_r), the size effect parameter (γ) and the stiffness of the elastic connectors to the (β_{eff}) on the natural frequency values of the elastically connected FG micro-panels. The next set of analyses employs the non-dimensional natural frequency written in the form $\lambda_{pq} = \omega_{pq}(a^2/h)\sqrt{\rho_m/E_m}$, which happens to be the standard non-dimensional form of the natural frequency for FG plate-like structure. Moreover, for quantitative measures of the degree of influence of some of the parameters (especially, the material length scale and the gradient index), two normalised frequency parameters are defined as:

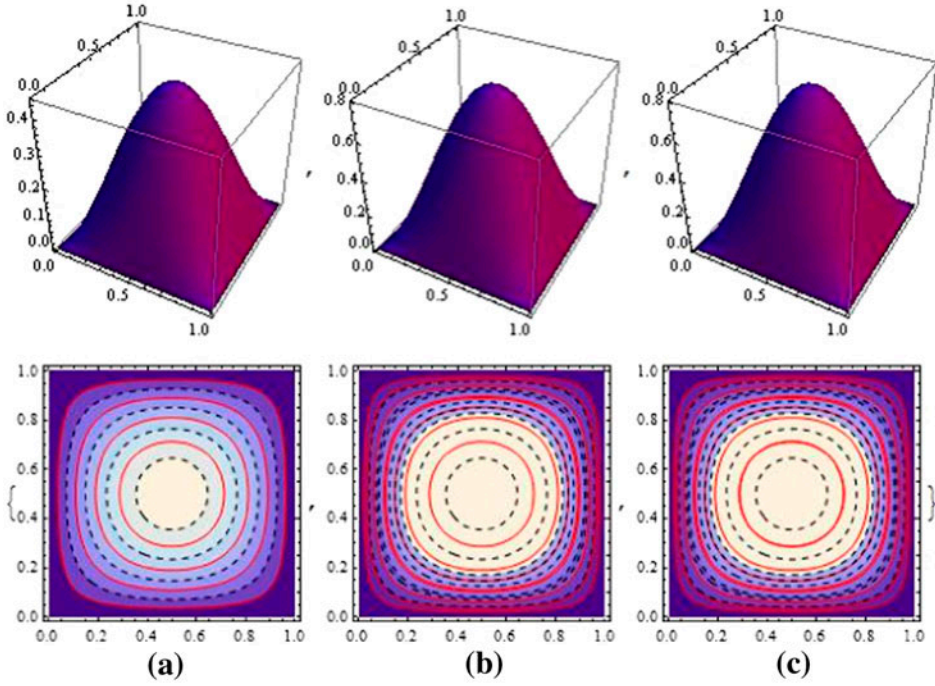


Figure 5. The vibration mode shape (upper) and the contour plot (lower) of λ_{11} : (a) $n = 0$; (b) $n = .5$; and (c) $n = 1$.

$$K_{pq} = \frac{(\lambda_{pq})_{FGP-EC}}{(\lambda_{pq})_{NFGP-EC}} \quad (54)$$

$$M_{pq} = \frac{(\lambda_{pq})_{FGP-EC}}{(\lambda_{pq})_{FGP-NEC}} \quad (55)$$

where in Equation (54), the term $(\lambda_{pq})_{FGP-EC}$ is the natural frequency of the elastically connected FG micro-panels, while $(\lambda_{nm})_{NFGP}$ is the natural frequency of the elastically connected non-FG micro-panels. The second ratio relates (M_{pq}) relates $(\lambda_{pq})_{FGP-EC}$ with $(\lambda_{pq})_{FGP-NEC}$ (which is the natural frequency of the *non-elastically* connected system with FG micro-panels).

Figure 8–12 demonstrates the variation of the natural frequency values related to the asynchronous motion of the coupled system. For brevity sake, all of the plots in Figure 8–11 correspond to the coupled system with the micro-panels made of polymer matrix FG with boron nitride. Specifically, Figure 8 reveals the variation of the normalised natural frequency (K_{11}) with respect to the span-to-thickness ratio (α) for four different values of the gradient index (n). The other parameters are taken as: $\beta_{eff} = 50$, $\gamma = 0$, $\phi = 1$. From this plot, it is seen that increased values of the span-to-thickness ratio leads only to a negligibly marginal increase in the natural frequency, under a constant value of the gradient index. However, for a given value of the span-to-width ratio, the magnitude of the natural frequency is found to decrease substantially with increasing value of the gradient index.

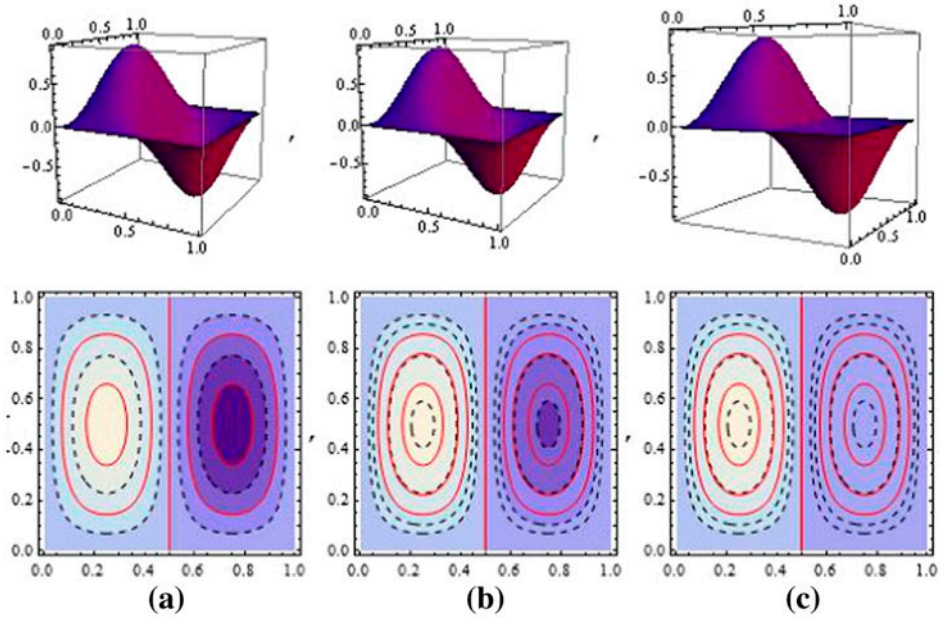


Figure 6. The vibration mode shape (upper) and the contour plot (lower) of λ_{12} : (a) $n = 0$; (b) $n = .5$; and (c) $n = 1$.

Figure 9 shows the influence of the effective stiffness (contributed by the elastic connectors) to the relationship between the frequency parameter and the gradient index. This plot illustrates the expected stiffening effect of the elastic connectors. It would be noticed that Figure 9 involves the normalised frequency (M_{pq}), with a focus on M_{11} and M_{22} . A few observations can be made from Figure 9. One of these observations is that the elastic connectors generate a quasi-quadratic incremental effect on the frequency-gradient index relationship, when the gradient index falls in the range $0 < n \leq 3$. However, a linear incremental effect is observed when the gradient index is in the range $3 \leq n < \infty$, where $n = \infty$ results in a structure with a homogeneous polymeric matrix phase. The other observation is that, since the elastic connectors are of finite stiffness when compared with the bending rigidity of each micro-panel, the increase in the value of the natural frequency caused by the effective stiffness of the elastic connectors is non-monotonic. This is highlighted in Figure 9(b), where it is seen that at the higher vibration mode, the percentage increase in the frequency value, caused by different value of the effective stiffness of the elastic connector, approaches each other. In Figure 10, the effect of the aspect ratio (ϕ) on the natural frequency–gradient index relationship is noticed to be very small under the two vibration modes considered. Moreover, an increasing trend in the frequency value is also found to accompany higher aspect ratio.

Figure 11 illustrates the influence of the size effect as the thickness value reduces. The size effect parameter considered falls in the range $.1 < \gamma \leq .9$. It would be recalled that the size effect parameter γ is defined as ζ/h . Thus, given the estimated value of the material length scale (ζ) for epoxy to be $17.6\mu\text{m}$, then the thickness values that correspond to the size effect parameter considered is in the range $170 \leq h \leq 20$. With this

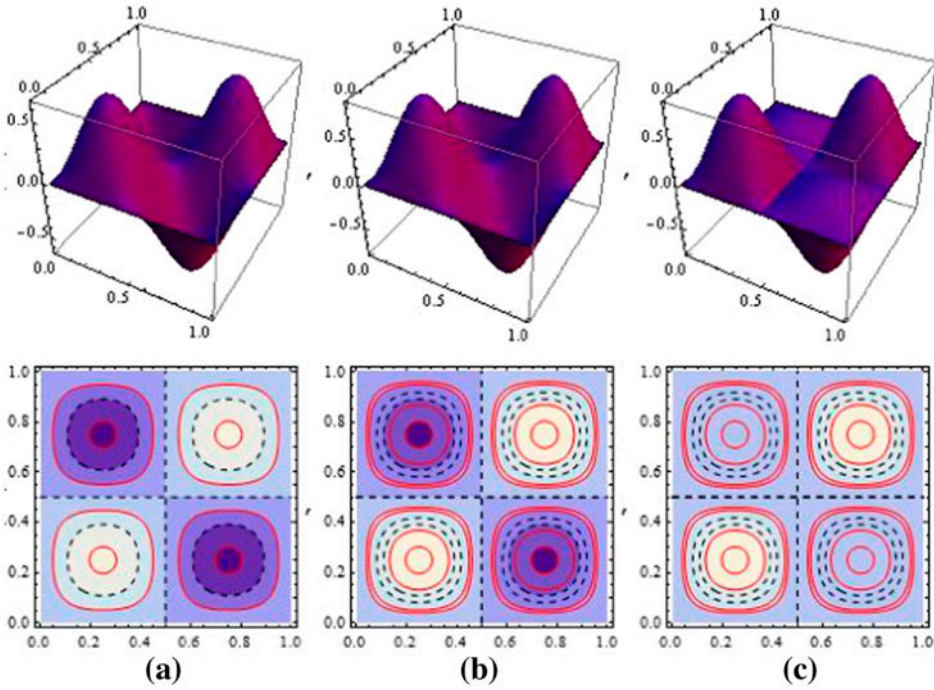


Figure 7. The vibration mode shape (upper) and the contour plot (lower) of λ_{22} : (a) $n = 0$; (b) $n = .5$; and (c) $n = 1$.

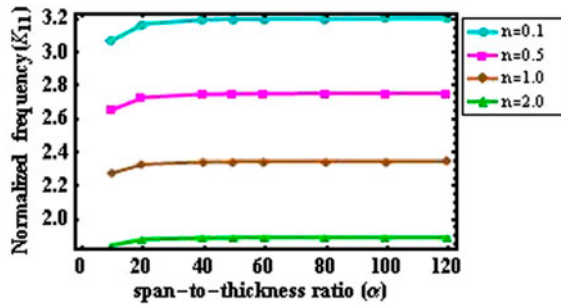


Figure 8. Variation of the normalised frequency of the asynchronous motion with respect to the span-to-width ratio for different values of the gradient index.

range of thickness value, the influence of the size effect is then evaluated on the system with FG micro-panels having aspect ratios of 1, effective stiffness value of 50 and a span-to-thickness value of 100. The observation from the two plots (Figure 11(a) and (b)) reveal that the low value of the gradient index (especially $n = .5$) contributes most significantly to the increase in the natural frequency, for a particular size effect. It is also seen that the incremental influence of the size effect decreases with increase in the thickness of the connected micro-panels. Figure 12 shows the sensitivity of the frequency parameter of the asynchronous motion of the coupled system at higher

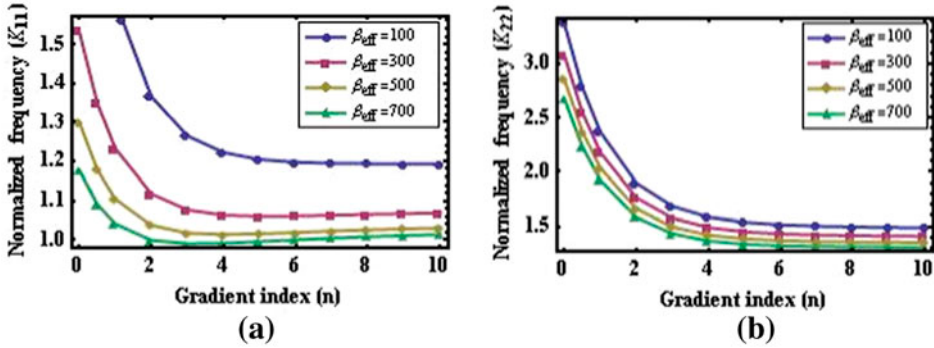


Figure 9. Influence of the effective stiffness of the elastic connectors on the frequency parameter: (a) with respect to K_{11} ; (b) with respect to K_{22} .

half-wave numbers. By comparing the four plots in Figure 12, one notices that of all the parameters, it is the size effect parameter that has a substantially noticeable effect at the higher frequency modes.

Figures 13–15 feature further illustration of the changes in the dynamic behaviour of the system. Essentially, these plots are meant to complement the analysis results presented in Figures 8–12. In these plots, examination of the influence of the material properties (Young’s modulus and density ratios) on the changes in the natural frequencies of the asynchronous motion of the elastically connected system is investigated. By focusing on the property of the two materials (provided in Table 1), we evaluate: (i) the distribution of the normalised natural frequencies for mode 1 under different gradient index (shown Figure 13); (ii) the distribution of the normalised natural frequencies for different aspect ratio in Figure 14; and (iii) the distribution of the normalised natural frequencies for different aspect ratio in Figure 15. In each plot, comparison is made between the normalised natural frequency of the system with micro-panels consisting of epoxy-boron nitride combination and epoxy-silicon carbide combination. It is seen from Figure 13, that for all values of gradient index, the average natural frequency of the system with epoxy-silicon carbide is higher than that consisting of epoxy-boron

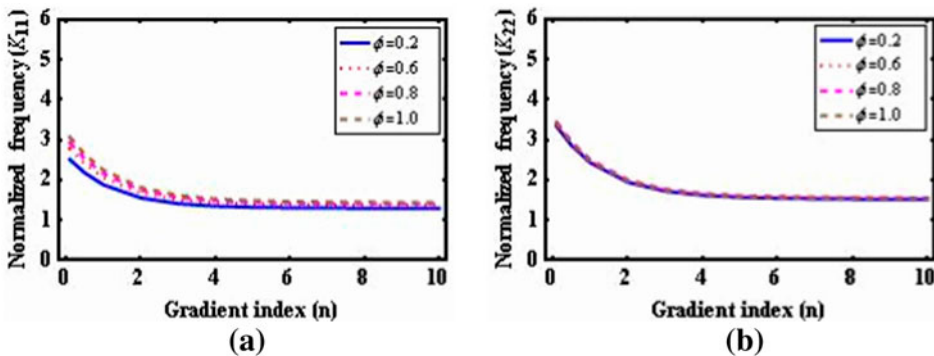


Figure 10. Effect of aspect ratio on the relationship between the natural frequency–gradient index relation of the asynchronous motion of the FG micro-panel system: (a) λ_{11} ; (b) λ_{22} .

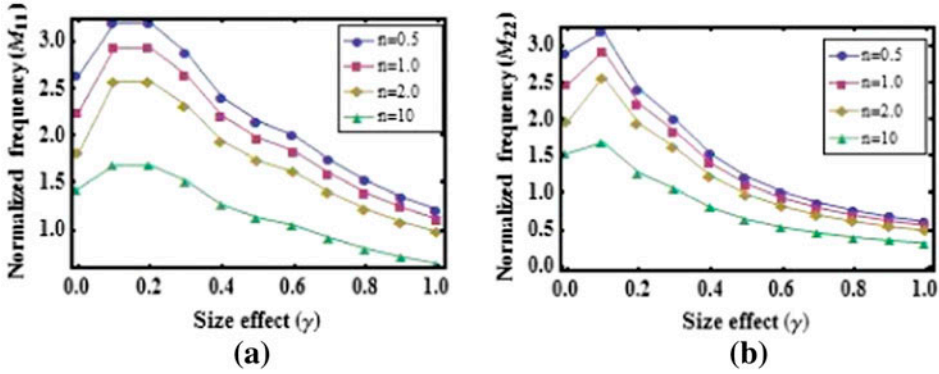


Figure 11. Effect of gradient index on the relationship between the natural frequency and the size effect: (a) λ_{11} ; (b) λ_{22} .

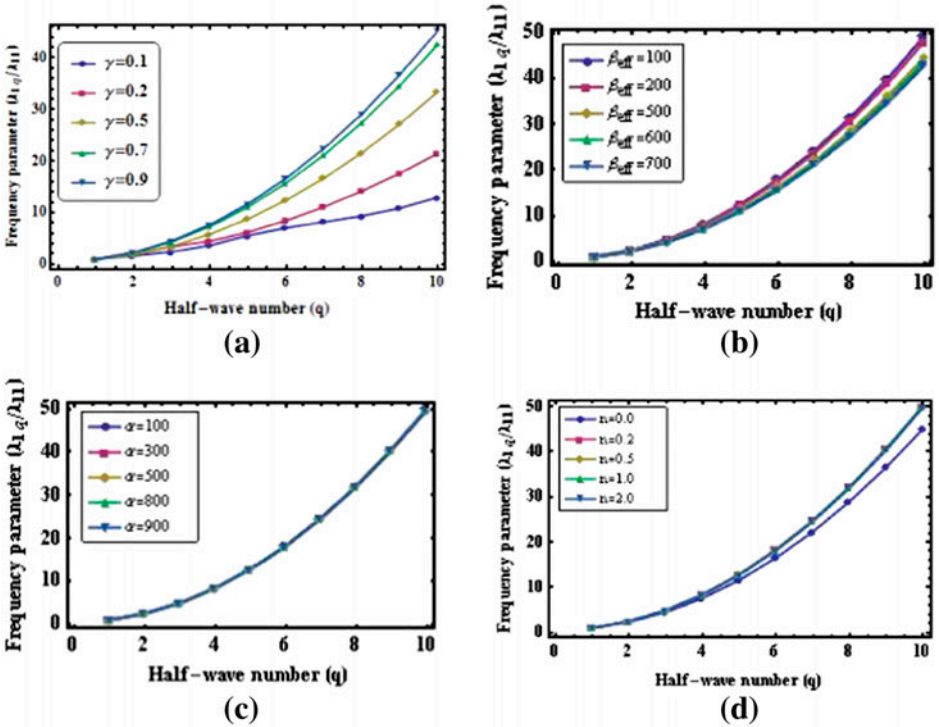


Figure 12. Sensitivity of the frequency parameter of the asynchronous motion of the coupled system at higher half-wave numbers: (a) influence of the material length scale; (b) influence of connectors' effective stiffness; (c) effect of span-to-thickness ratio; and (d) influence of the gradient index.

nitride combination, with the difference getting higher as the gradient index increases. With respect to the variation of the aspect ratio, it is noticed from Figure 14 that the average natural frequency of the system with epoxy-silicon carbide is again higher. In

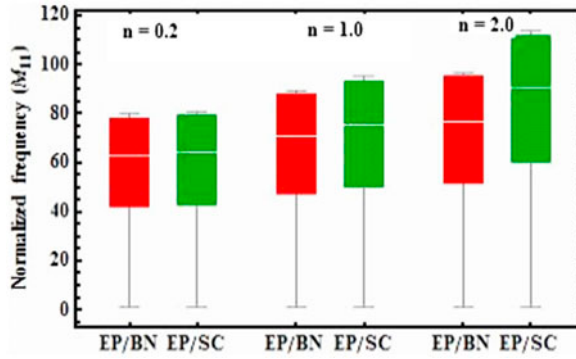


Figure 13. Distribution of the normalised natural frequencies for the mode 1 for different gradient index.

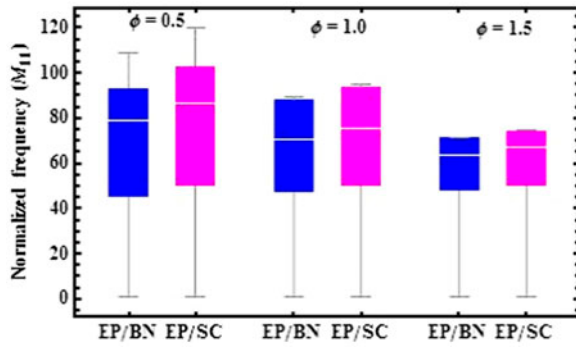


Figure 14. Distribution of the normalised natural frequencies for mode 1 for different aspect ratios.

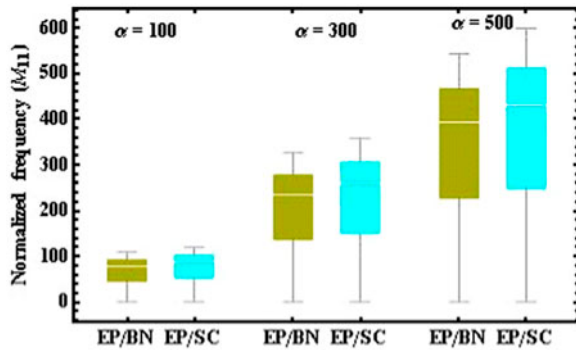


Figure 15. Distribution of the normalised natural frequencies for mode 1 for different span-to-thickness ratios.

Figure 15, the distribution of the frequency parameter is evaluated under the variation of the span-to-thickness ratio. This plot shows that at the lower values of the span-to-thickness ratio, the distribution of the frequency is quite similar for the two material properties. Additionally, increasing values of the span-to-thickness ratio further reveals a glaring difference between the frequency values of the epoxy-silicon carbide combination and the epoxy-boron nitride combination. The behaviours noticed from Figure 13–15 seem to be consistent with the fact that the epoxy-silicon carbide combination provides a very high value of the Young's modulus ratio.

6. Conclusion

The free vibratory behaviour of a system of elastically connected micro-panels is studied. The behaviour analyses were predicated on a set of biharmonic governing equations derived from a combination of the energy method, postulates of the Kirchhoff–Love theory of thin plate and the constitutive rule of the MCST. The formulation procedure yields a system of three field equations representing the motion of the system in a Cartesian system of coordinates. The three field equations were cast into non-dimensional forms to reduce the dimensionality of the mathematical model. As a result, seven non-dimensional variables emerged and they are used to examine the variation of the dynamic behaviour as a result of changes to: (a) geometric parameters of the FG micro-panel; (b) the materials properties of the FG-micro-panels; and (c) the effective stiffness of the elastic connectors. The free vibration behaviour of the coupled FG micro-scale panels were investigated in terms of the out-of-phase motion of the coupled FG micro-panel via the Navier method of solution. The analyses revealed that: (i) the ratio of the constituents Young's modulus imposes a higher degree of stiffening effect to the vibration of the system than the stiffness of the elastic connectors and the density ratio of the constituent materials; (ii) the influence of the size effect is more pronounced as the thickness of the FG micro-panel is reduced; (iii) the effect of the increase in the gradient index is reduced by the presence of the size effect; and (iv) the effect of the span-to-thickness ratio on the natural frequency of the system is reduced for lower values of the gradient index and higher values of the half-wave number.

Disclosure statement

No potential conflict of interest was reported by the author.

ORCID

K.B. Mustapha  <http://orcid.org/0000-0002-9905-9162>

References

- Abbasi, M., & Mohammadi, A. K. (2013, October). Study of the sensitivity and resonant frequency of the flexural modes of an atomic force microscopy microcantilever modeled by strain gradient elasticity theory. *Proceedings of the Institution of Mechanical Engineers, Part C: Journal of Mechanical Engineering Science*, 228, 1299–1310.
- Aifantis, E. C. (1984). On the microstructural origin of certain inelastic models. *Journal of Engineering Materials and Technology*, 106, 326–330.
- Aifantis, E. C. (1992). On the role of gradients in the localization of deformation and fracture. *International Journal of Engineering Science*, 30, 1279–1299.

- Akgöz, B., & Civalek, Ö. (2013a). Free vibration analysis of axially functionally graded tapered Bernoulli–Euler microbeams based on the modified couple stress theory. *Composite Structures*, 98, 314–322.
- Akgöz, B., & Civalek, Ö. (2013b). Longitudinal vibration analysis of strain gradient bars made of functionally graded materials (FGM). *Composites Part B: Engineering*, 55, 263–268.
- Akgöz, B., & Civalek, Ö. (2013c). Modeling and analysis of micro-sized plates resting on elastic medium using the modified couple stress theory. *Meccanica*, 48, 863–873.
- Anthoine, A. (2000). Effect of couple-stresses on the elastic bending of beams. *International Journal of Solids and Structures*, 37, 1003–1018.
- Arani, A. G., Kolahchi, R., Barzoki, A. A. M., Mozdianfard, M. R., & Farahani, S. M. N. (2012). Elastic foundation effect on nonlinear thermo-vibration of embedded double layered orthotropic graphene sheets using differential quadrature method. *Proceedings of the Institution of Mechanical Engineers Part C: Journal of Mechanical Engineering Science*, 227, 862–879.
- Asghari, M., Ahmadian, M. T., Kahrobaiyan, M. H., & Rahaeifard, M. (2010). On the size-dependent behavior of functionally graded micro-beams. *Materials & Design*, 31, 2324–2329.
- Baferani, A. H., Saidi, A. R., & Jomehzadeh, E. (2011). An exact solution for free vibration of thin functionally graded rectangular plates. *Proceedings of the Institution of Mechanical Engineers, Part C: Journal of Mechanical Engineering Science*, 225, 526–536.
- Benatta, M. A., Mechab, I., Tounsi, A., & Adda Bedia, E. A. (2008). Static analysis of functionally graded short beams including warping and shear deformation effects. *Computational Materials Science*, 44, 765–773.
- Boss, J. N., & Ganesh, V. K. (2006). Fabrication and properties of graded composite rods for biomedical applications. *Composite Structures*, 74, 289–293.
- Chakraborty, A., Gopalakrishnan, S., & Reddy, J. N. (2003). A new beam finite element for the analysis of functionally graded materials. *International Journal of Mechanical Sciences*, 45, 519–539.
- Challamel, N. (2013). Variational formulation of gradient or/and nonlocal higher-order shear elasticity beams. *Composite Structures*, 105, 351–368.
- Choi, Y. H., Bulliard, X., Benayad, A., Leterrier, Y., Månson, J. A. E., Lee, K. H., ... Kim, J. (2010). Design and fabrication of compositionally graded inorganic oxide thin films: Mechanical, optical and permeation characteristics. *Acta Materialia*, 58, 6495–6503.
- Cosserat E. C. F. (1909). *Théorie des Corps Déformables* [Theory of deformable bodies]. Paris: A. Hermann et Fils.
- Daouadji, T., Henni, A., Tounsi, A., & El Abbes, A. (2013). Elasticity solution of a cantilever functionally graded beam. *Applied Composite Materials*, 20, 1–15.
- Elishakoff, I. (2005). *Eigenvalues of inhomogeneous structures: Unusual closed-form solutions*. Boca Raton, FL: CRC Press.
- Erdogan, F. (1995). Fracture mechanics of functionally graded materials. *Composites Engineering*, 5, 753–770.
- Fleck, N. A., & Hutchinson, J. W. (1993). A phenomenological theory for strain gradient effects in plasticity. *Journal of the Mechanics and Physics of Solids*, 41, 1825–1857.
- Fleck, N. A., Muller, G. M., Ashby, M. F., & Hutchinson, J. W. (1994). Strain gradient plasticity: Theory and experiment. *Acta Metallurgica et Materialia*, 42, 475–487.
- Gao, X. L., Huang, J. X., Reddy, J. N. (2013). A non-classical third-order shear deformation plate model based on a modified couple stress theory. *Acta Mechanica*, 224, 2699–2718.
- Jin, Z. H., & Batra, R. C. (1996). Some basic fracture mechanics concepts in functionally graded materials. *Journal of the Mechanics and Physics of Solids*, 44, 1221–1235.
- Jomehzadeh, E., Noori, H. R., & Saidi, A. R. (2011). The size-dependent vibration analysis of micro-plates based on a modified couple stress theory. *Physica E: Low-dimensional Systems and Nanostructures*, 43, 877–883.
- Ke, L.-L., Wang, Y.-S., Yang, J., & Kitipornchai, S. (2012). Free vibration of size-dependent mindlin microplates based on the modified couple stress theory. *Journal of Sound and Vibration*, 331, 94–106.
- Koizumi, M. (1992). *Ceramic transactions, functionally gradient materials* (Vol. 34). Westerville, OH: The American Ceramic Society.
- Krumova, M., Klingshirn, C., Hauptert, F., & Friedrich, K. (2001). Microhardness studies on functionally graded polymer composites. *Composites Science and Technology*, 61, 557–563.

- Kun, W., & Nguyen, C. T. C. (1999). High-order medium frequency micromechanical electronic filters. *Journal of Microelectromechanical Systems*, 8, 534–556.
- Lam, D. C. C., Yang, F., Chong, A. C. M., Wang, J., & Tong, P. (2003). Experiments and theory in strain gradient elasticity. *Journal of the Mechanics and Physics of Solids*, 51, 1477–1508.
- Lekhnitskii, S. G. (1977). *Theory of the elasticity of anisotropic bodies*. San Francisco, CA: Mir.
- Li, Y.-H., & Su, Y.-C. (2010). Miniature osmotic actuators for controlled maxillofacial distraction osteogenesis. *Journal of Micromechanics and Microengineering*, 20, 065013.
- Liu, Y., & Shu, D. W. (2014). Free vibration analysis of exponential functionally graded beams with a single delamination. *Composites Part B: Engineering*, 59, 166–172.
- Liu, T., Wang, Q., Gao, A., Zhang, C., Wang, C., & He, J. (2007). Fabrication of functionally graded materials by a semi-solid forming process under magnetic field gradients. *Scripta Materialia*, 57, 992–995.
- Maranganti, R., & Sharma, P. (2007). A novel atomistic approach to determine strain-gradient elasticity constants: Tabulation and comparison for various metals, semiconductors, silica, polymers and the (Ir) relevance for nanotechnologies. *Journal of the Mechanics and Physics of Solids*, 55, 1823–1852.
- Mattila, T., Kiihamäki, J., Lamminmäki, T., Jaakkola, O., Rantakari, P., Oja, A., ... Tittonen, I. (2002). A 12 0MHz micromechanical bulk acoustic mode oscillator. *Sensors and Actuators A: Physical*, 101, 1–9.
- Mindlin, R. D., & Tiersten, H. F. (1962). Effects of couple-stresses in linear elasticity. *Archive for Rational Mechanics and Analysis*, 11, 415–448.
- Mohammadi, M., Saidi, A., & Jomehzadeh, E. (2010). Levy solution for buckling analysis of functionally graded rectangular plates. *Applied Composite Materials*, 17, 81–93.
- Murmu, T., & Adhikari, S. (2011). Nonlocal vibration of bonded double-nanoplate-systems. *Composites Part B: Engineering*, 42, 1901–1911.
- Mustapha, K. B., & Zhong, Z. W. (2012a). Spectral element analysis of a non-classical model of a spinning micro beam embedded in an elastic medium. *Mechanism and Machine Theory*, 53, 66–85.
- Mustapha, K. B., & Zhong, Z. W. (2012b). Wave propagation characteristics of a twisted micro scale beam. *International Journal of Engineering Science*, 53, 46–57.
- Nguyen, C. T. C. (1995). Micromechanical resonators for oscillators and filters. In *Ultrasonics symposium. Proceedings of the 1995 IEEE* (Vol. 1, pp. 489–499). Seattle, WA.
- Omori, M., Kakita, T., Okubo, A., & Hirai, T. (1999). Pure WC/Mo functionally graded materials. *Materials Science Forum*, 308–311, 53–58.
- Papargyri-Beskou, S., Tsepoura, K. G., Polyzos, D., & Beskos, D. E. (2003). Bending and stability analysis of gradient elastic beams. *International Journal of Solids and Structures*, 40, 385–400.
- Park, S. K., & Gao, X. L. (2006). Bernoulli–Euler beam model based on a modified couple stress theory. *Journal of Micromechanics and Microengineering*, 16, 2355–2359.
- Ravichandran, K. S. (1995). Thermal residual stresses in a functionally graded material system. *Materials Science and Engineering A*, 201, 269–276.
- Reddy, J. N. (2002). *Energy principles and variational methods in applied mechanics* (2nd ed.). Hoboken, NJ: Wiley.
- Reddy, J. N. (2011). Microstructure-dependent couple stress theories of functionally graded beams. *Journal of the Mechanics and Physics of Solids*, 59, 2382–2399.
- Reddy, J. N., & Chin, C. D. (1998). Thermomechanical analysis of functionally graded cylinders and plates. *Journal of Thermal Stresses*, 21, 593–626.
- Saliterman, S. (2006). *Fundamentals of BioMEMS and medical microdevices* (Vol. 153). Bellingham, WA: SPIE Press.
- Shackelford, J. F., & Alexander, W. (2000). Mechanical properties of materials. In *CRC materials science and engineering handbook* (3rd ed.). Boca Raton, FL: CRC Press.
- Sharma, V., & Kumar, S. (2013). Velocity dispersion in an elastic plate with microstructure: Effects of characteristic length in a couple stress model. *Meccanica*, 49, 1083–1090.
- Shaw, L. L. (1998). Thermal residual stresses in plates and coatings composed of multi-layered and functionally graded materials. *Composites Part B: Engineering*, 29, 199–210.
- Shen, H.-S. (2002). Postbuckling analysis of axially-loaded functionally graded cylindrical shells in thermal environments. *Composites Science and Technology*, 62, 977–987.

- Şimşek, M. (2009). Static analysis of a functionally graded beam under a uniformly distributed load by Ritz method. *International Journal of Engineering and Applied Sciences*, 1, 1–11.
- Şimşek, M., Kocatürk, T., & Akbaş, Ş. D. (2012). Dynamic behavior of an axially functionally graded beam under action of a moving harmonic load. *Composite Structures*, 94, 2358–2364.
- Subra Suresh, A. M. (1998). *Fundamentals of functionally graded materials: Processing and thermomechanical behaviour of graded metals and metal-ceramic composites*. London: IOM Communications Ltd.
- Sur, A., & Kanoria, M. (2014). Thermoelastic interaction in a viscoelastic functionally graded half-space under three-phase-lag model. *European Journal of Computational Mechanics*, 23, 179–198.
- Suresh, S., & Mortensen, A. (1997). Functionally graded metals and metal-ceramic composites: Part 2 thermomechanical behaviour. *International Materials Reviews*, 42, 85–116.
- Szillard, R. (2004). *Theories and applications of plate analysis*. Hoboken, NJ: Wiley.
- Teixeira, V., Andritschky, M., & Stöver, D. (1999). Modelling of thermal residual stresses in graded ceramic coatings. *Materials Science Forum*, 308–311, 930–935.
- Thai, H.-T., & Kim, S.-E. (2013). Closed-form solution for buckling analysis of thick functionally graded plates on elastic foundation. *International Journal of Mechanical Sciences*, 75, 34–44.
- Thai, H.-T., & Uy, B. (2013). Levy solution for buckling analysis of functionally graded plates based on a refined plate theory. *Proceedings of the Institution of Mechanical Engineers, Part C: Journal of Mechanical Engineering Science*, 227, 2649–2664.
- Thai, H.-T., & Vo, T. P. (2013). A size-dependent functionally graded sinusoidal plate model based on a modified couple stress theory. *Composite Structures*, 96, 376–383.
- Toupin, R. A. (1964). Theories of elasticity with couple-stress. *Archive for Rational Mechanics and Analysis*, 17, 85–112.
- Wang, L., Liu, H. T., Ni, Q., & Wu, Y. (2013). Flexural vibrations of microscale pipes conveying fluid by considering the size effects of micro-flow and micro-structure. *International Journal of Engineering Science*, 71, 92–101.
- Xiang, H. J., & Yang, J. (2008). Free and forced vibration of a laminated FGM Timoshenko beam of variable thickness under heat conduction. *Composites Part B: Engineering*, 39, 292–303.
- Yang, F., Chong, A. C. M., Lam, D. C. C., Tong, P. (2002). Couple stress based strain gradient theory for elasticity. *International Journal of Solids and Structures*, 39, 2731–2743.
- Yazdi, N., Ayazi, F., & Najafi, K. (1998). Micromachined inertial sensors. *Proceedings of the IEEE*, 86, 1640–1659.
- Yin, L., Qian, Q., Wang, L., & Xia, W. (2010). Vibration analysis of microscale plates based on modified couple stress theory. *Acta Mechanica Solida Sinica*, 23, 386–393.
- Ying, J., Lü, C. F., & Chen, W. Q. (2008). Two-dimensional elasticity solutions for functionally graded beams resting on elastic foundations. *Composite Structures*, 84, 209–219.
- Zhang, B., He, Y., Liu, D., Gan, Z., & Shen, L. (2013). A novel size-dependent functionally graded curved microbeam model based on the strain gradient elasticity theory. *Composite Structures*, 106, 374–392.
- Zhou, Z.-G., Wang, B. (2006). Non-local theory solution for an anti-plane shear permeable crack in functionally graded piezoelectric materials. *Applied Composite Materials*, 13, 345–367.

Appendix 1

$$\tau_{xx} = \frac{E(z)}{(1-\nu^2)} \left[\frac{\partial u}{\partial x} - z \frac{\partial^2 w}{\partial x^2} + \nu \left(\frac{\partial v}{\partial y} - z \frac{\partial^2 w}{\partial y^2} \right) \right] \quad (\text{A1})$$

$$\tau_{yy} = \frac{E(z)}{(1-\nu^2)} \left[\frac{\partial v}{\partial y} - z \frac{\partial^2 w}{\partial y^2} + \nu \left(\frac{\partial u}{\partial x} - z \frac{\partial^2 w}{\partial x^2} \right) \right] \quad (\text{A2})$$

$$\tau_{xy} = \frac{E(z)}{(1+\nu)} \left[\frac{1}{2} \frac{\partial u}{\partial y} + \frac{1}{2} \frac{\partial v}{\partial x} - z \frac{\partial^2 w}{\partial y \partial x} \right] \quad (\text{A3})$$

$$m_{xx} = -m_{yy} = 2G(z)\zeta^2 \frac{\partial^2 w}{\partial y \partial x} \quad (\text{A4})$$

$$m_{xy} = G(z)\zeta^2 \left[-\frac{\partial^2 w}{\partial x^2} + \frac{\partial^2 w}{\partial y^2} \right] \quad (\text{A5})$$

$$m_{zx} = \frac{G(z)\zeta^2}{2} \left[-\frac{\partial^2 u}{\partial y^2} + \frac{\partial^2 v}{\partial y \partial x} \right] \quad (\text{A6})$$

$$m_{zy} = \frac{G(z)\zeta^2}{2} \left[-\frac{\partial^2 u}{\partial y \partial x} + \frac{\partial^2 v}{\partial x^2} \right] \quad (\text{A7})$$

$$A_1 = \frac{h\rho_m(n + \rho_r)}{1 + n}; \quad A_2 = \frac{hE_m(n + E_r)}{2(1 + n)(1 + v)}; \quad A_3 = \frac{h\zeta^2 E_m(n + E_r)}{8(1 + n)(1 + v)} \quad (\text{A8})$$

$$A_4 = \frac{h^2 n \rho_m(-1 + \rho_r)}{2(1 + n)(2 + n)}; \quad A_5 = \frac{hE_m(n + E_r)}{2(1 + n)(-1 + v)}; \quad A_6 = \frac{h^2 n E_m(-1 + E_r)}{2(1 + n)(2 + n)(-1 + v)(1 + v)} \quad (\text{A9})$$

$$A_7 = \frac{h\zeta^2 E_m(n + E_r)}{8(1 + n)(1 + v)}; \quad A_8 = \frac{hE_m(n + E_r)}{(1 + n)(-1 + v)(1 + v)}; \quad A_9 = \frac{h\zeta^2 E_e(n + E_r)}{8(1 + n)(1 + v)} \quad (\text{A10})$$

$$A_{10} = \frac{h^2 n E_m(-1 + E_r)}{2(1 + n)(2 + n)(-1 + v)(1 + v)}; \quad A_{11} = \frac{h\zeta^2 E_m(n + E_r)}{8(1 + n)(1 + v)} \quad (\text{A11})$$

$$B_1 = -\frac{h\rho_m(n + \rho_r)}{1 + n}; \quad B_2 = \frac{h^2 n \rho_m(-1 + \rho_r)}{2(1 + n)(2 + n)}; \quad B_3 = \frac{hE_m(n + E_r)}{(1 + n)(-1 + v)(1 + v)} \quad (\text{A12})$$

$$B_4 = \frac{h^2 n E_m(-1 + E_r)}{2(1 + n)(2 + n)(-1 + v)(1 + v)}; \quad B_5 = \frac{hE_m(n + E_r)}{2(1 + n)(-1 + v)}; \quad B_6 = \frac{h\zeta^2 E_m(n + E_r)}{8(1 + n)(1 + v)} \quad (\text{A13})$$

$$B_7 = \frac{hE_m(n + E_r)}{2(1 + n)(1 + v)}; \quad B_8 = \frac{h^2 n E_m(-1 + E_r)}{2(1 + n)(2 + n)(-1 + v)(1 + v)}; \quad B_9 = \frac{h\zeta^2 E_m(n + E_r)}{8(1 + n)(1 + v)} \quad (\text{A14})$$

$$B_{10} = \frac{h\zeta^2 E_m(n + E_r)}{8(1 + n)(1 + v)}; \quad B_{11} = \frac{h\zeta^2 E_m(n + E_r)}{8(1 + n)(1 + v)} \quad (\text{A15})$$

$$C_1 = -\frac{h\rho_m(n + \rho_r)}{1 + n}; \quad C_2 = \frac{h^2 n \rho_m(-1 + \rho_r)}{2(1 + n)(2 + n)}; \quad C_3 = \frac{h^3 \rho_m(n^3 + 6\rho_r + 3n^2(1 + \rho_r) + n(8 + 3\rho_r))}{12(1 + n)(2 + n)(3 + n)} \quad (\text{A16})$$

$$C_4 = \frac{h^2 n E_e(-1 + E_r)}{2(1 + n)(2 + n)(-1 + v)(1 + v)}; \quad C_5 = \frac{h^2 n \rho_m(-1 + \rho_r)}{2(1 + n)(2 + n)} \quad (\text{A17})$$

$$C_6 = \frac{h^2 n E e_m (-1 + E e_r)}{2(1+n)(2+n)(-1+v)(1+v)}; \quad (A18)$$

$$C_7 = \frac{h^3 \rho_m (n^3 + 6\rho_r + 3n^2(1 + \rho_r) + n(8 + 3\rho_r))}{12(1+n)(2+n)(3+n)}$$

$$C_8 = \frac{h^2 n E e_m (-1 + E e_r)}{2(1+n)(2+n)(-1+v)(1+v)}; \quad C_9 = \frac{h^2 n E e_m (-1 + E e_r)}{2(1+n)(2+n)(-1+v)(1+v)} \quad (A19)$$

$$C_{10} = \left[\frac{h(h^2(2+n+n^2) - 2(6+5n+n^2)\zeta^2(-1+v))E e_m E e_r}{4(1+n)(2+n)(3+n)(-1+v)(1+v)} \right. \\ \left. + \frac{h\zeta^2 E e_m (-12n(6+5n+n^2)(-1+v) - 12(6+5n+n^2)(-1+v)E e_r)}{24(1+n)(2+n)(3+n)(-1+v)(1+v)} \right] \quad (A20)$$

$$C_{11} = \left[\frac{h(h^2(2+n+n^2) - 2(6+5n+n^2)\zeta^2(-1+v))E e_m E e_r}{2(1+n)(2+n)(3+n)(-1+v)(1+v)} \right. \\ \left. + \frac{h\zeta^2 E e_m (-12n(6+5n+n^2)(-1+v) - 12(6+5n+n^2)(-1+v)E e_r)}{12(1+n)(2+n)(3+n)(-1+v)(1+v)} \right] \quad (A21)$$

$$C_{12} = \left[\frac{h(h^2(2+n+n^2) - 2(6+5n+n^2)\zeta^2(-1+v))E e_m E e_r}{4(1+n)(2+n)(3+n)(-1+v)(1+v)} \right. \\ \left. + \frac{h\zeta^2 E e_m (-12n(6+5n+n^2)(-1+v) - 12(6+5n+n^2)(-1+v)E e_r)}{24(1+n)(2+n)(3+n)(-1+v)(1+v)} \right] \quad (A22)$$

$$Q_1 = \left[-\frac{h(n + E_r)}{2(1+n)(1+v)} + \frac{h^3(2+n+n^2)E_m}{4(1+n)(2+n)(3+n)(-1+v)(1+v)} \right] \quad (A23)$$

$$Q_2 = \left[-\frac{h(n + E_r)}{(1+n)(1+v)} + \frac{h^3(2+n+n^2)E_m}{2(1+n)(2+n)(3+n)(-1+v)(1+v)} \right] \quad (A24)$$

$$Q_3 = \left[-\frac{h(n + E_r)}{2(1+n)(1+v)} + \frac{h^3(2+n+n^2)E_m}{4(1+n)(2+n)(3+n)(-1+v)(1+v)} \right] \quad (A25)$$

$$W_{11} = \frac{12p^2\pi^2\alpha^2(1-v^2)(n + E e_r)}{(1+n)(-1+v)(1+v)} - \frac{6\pi^2q^2\alpha^2(1-v^2)\phi^2(n + E e_r)}{(1+n)(1+v)} \\ - \frac{3p^2\pi^4q^2\alpha^2\gamma^2(1-v^2)\phi^2(n + E e_r)}{2(1+n)(1+v)} - \frac{3\pi^4q^4\alpha^2\gamma^2(1-v^2)\phi^4(n + E e_r)}{2(1+n)(1+v)} \\ + \frac{\lambda_{pq}^2(n + \rho_r)}{1+n} \quad (A26)$$

$$W_{12} = \frac{6p\pi^2q\alpha^2(1-v^2)\phi(n + E_r)}{(1+n)(-1+v)} + \frac{3p^3\pi^4q\alpha^2\gamma^2(1-v^2)\phi(n + E_r)}{2(1+n)(1+v)} \\ + \frac{3p\pi^4q^3\alpha^2\gamma^2(1-v^2)\phi^3(n + E_r)}{2(1+n)(1+v)} \quad (A27)$$

$$W_{13} = -\frac{6np^3\pi^3\alpha(1-v^2)(-1+Ee_r)}{(1+n)(2+n)(-1+v)(1+v)} - \frac{6np\pi^3q^2\alpha(1-v^2)\phi^2(-1+Ee_r)}{(1+n)(2+n)(-1+v)(1+v)} - \frac{6np\pi(1-v^2)\lambda_{pq}^2(-1+\rho_r)}{(1+n)(2+n)\alpha} \quad (\text{A28})$$

$$W_{21} = \frac{6p\pi^2q\alpha^2(1-v^2)\phi(n+Ee_r)}{(1+n)(-1+v)} + \frac{3p^3\pi^4q\alpha^2\gamma^2(1-v^2)\phi(n+Ee_r)}{2(1+n)(1+v)} + \frac{3p\pi^4q^3\alpha^2\gamma^2(1-v^2)\phi^3(n+Ee_r)}{2(1+n)(1+v)} \quad (\text{A29})$$

$$W_{22} = -\frac{6p^2\pi^2\alpha^2(1-v^2)(n+Ee_r)}{(1+n)(1+v)} - \frac{3p^4\pi^4\alpha^2\gamma^2(1-v^2)(n+Ee_r)}{2(1+n)(1+v)} - \frac{3p^2\pi^4q^2\alpha^2\gamma^2(1-v^2)\phi^2(n+Ee_r)}{2(1+n)(1+v)} + \frac{12\pi^2q^2\alpha^2(1-v^2)\phi^2(n+Ee_r)}{(1+n)(-1+v)(1+v)} + \frac{\lambda_{pq}^2(n+\rho_r)}{1+n} \quad (\text{A30})$$

$$W_{23} = -\frac{6np^2\pi^3q\alpha(1-v^2)\phi(-1+Ee_r)}{(1+n)(2+n)(-1+v)(1+v)} - \frac{6n\pi^3q^3\alpha(1-v^2)\phi^3(-1+Ee_r)}{(1+n)(2+n)(-1+v)(1+v)} - \frac{6n\pi q(1-v^2)\phi\lambda_{pq}^2(-1+\rho_r)}{(1+n)(2+n)\alpha} \quad (\text{A31})$$

$$W_{31} = -\frac{6np^3\pi^3\alpha(1-v^2)(-1+Ee_r)}{(1+n)(2+n)(-1+v)(1+v)} - \frac{6np\pi^3q^2\alpha(1-v^2)\phi^2(-1+Ee_r)}{(1+n)(2+n)(-1+v)(1+v)} - \frac{6np\pi(1-v^2)\lambda_{pq}^2(-1+\rho_r)}{(1+n)(2+n)\alpha} \quad (\text{A32})$$

$$W_{32} = -\frac{6np^2\pi^3q\alpha(1-v^2)\phi(-1+Ee_r)}{(1+n)(2+n)(-1+v)(1+v)} - \frac{6n\pi^3q^3\alpha(1-v^2)\phi^3(-1+Ee_r)}{(1+n)(2+n)(-1+v)(1+v)} - \frac{6n\pi q(1-v^2)\phi\lambda_{pq}^2(-1+\rho_r)}{(1+n)(2+n)\alpha} \quad (\text{A33})$$

$$W_{33} = \frac{\lambda_{pq}^2(n+\rho_r)}{1+n} + \frac{p^2\pi^2(1-v^2)\lambda_{pq}^2(n^3+6\rho_r+3n^2(1+\rho_r)+n(8+3\rho_r))}{(1+n)(2+n)(3+n)\alpha^2} + 2\beta_{\text{eff}} + W_{33a} + W_{33b} + W_{33c} \quad (\text{A34})$$

$$\begin{aligned}
W_{33a} = & -\frac{8n\pi^4 q^4 \phi^4}{(1+n)(2+n)(3+n)} - \frac{3n^2 \pi^4 q^4 \phi^4}{(1+n)(2+n)(3+n)} - \frac{n^3 \pi^4 q^4 \phi^4}{(1+n)(2+n)(3+n)} \\
& - \frac{36n\pi^4 q^4 \alpha^2 \gamma^2 \phi^4}{(1+n)(2+n)(3+n)} - \frac{30n^2 \pi^4 q^4 \alpha^2 \gamma^2 \phi^4}{(1+n)(2+n)(3+n)} - \frac{6n^3 \pi^4 q^4 \alpha^2 \gamma^2 \phi^4}{(1+n)(2+n)(3+n)} \\
& + \frac{36n\pi^4 q^4 \alpha^2 \gamma^2 v \phi^4}{(1+n)(2+n)(3+n)} + \frac{30n^2 \pi^4 q^4 \alpha^2 \gamma^2 v \phi^4}{(1+n)(2+n)(3+n)} + \frac{6n^3 \pi^4 q^4 \alpha^2 \gamma^2 v \phi^4}{(1+n)(2+n)(3+n)} \\
& - \frac{6\pi^4 q^4 \phi^4 E_r}{(1+n)(2+n)(3+n)} - \frac{3n\pi^4 q^4 \phi^4 E_r}{(1+n)(2+n)(3+n)} - \frac{3n^2 \pi^4 q^4 \phi^4 E_r}{(1+n)(2+n)(3+n)} \\
& - \frac{36\pi^4 q^4 \alpha^2 \gamma^2 \phi^4 E_r}{(1+n)(2+n)(3+n)} - \frac{30n\pi^4 q^4 \alpha^2 \gamma^2 \phi^4 E_r}{(1+n)(2+n)(3+n)} - \frac{6n^2 \pi^4 q^4 \alpha^2 \gamma^2 \phi^4 E_r}{(1+n)(2+n)(3+n)} \\
& + \frac{36\pi^4 q^4 \alpha^2 \gamma^2 v \phi^4 E_r}{(1+n)(2+n)(3+n)} + \frac{30n\pi^4 q^4 \alpha^2 \gamma^2 v \phi^4 E_r}{(1+n)(2+n)(3+n)} + \frac{6n^2 \pi^4 q^4 \alpha^2 \gamma^2 v \phi^4 E_r}{(1+n)(2+n)(3+n)}
\end{aligned} \tag{A35}$$

$$\begin{aligned}
W_{33b} = & -\frac{16np^2 \pi^4 q^2 \phi^2}{(1+n)(2+n)(3+n)} - \frac{6n^2 p^2 \pi^4 q^2 \phi^2}{(1+n)(2+n)(3+n)} - \frac{2n^3 p^2 \pi^4 q^2 \phi^2}{(1+n)(2+n)(3+n)} \\
& - \frac{72np^2 \pi^4 q^2 \alpha^2 \gamma^2 \phi^2}{(1+n)(2+n)(3+n)} - \frac{60n^2 p^2 \pi^4 q^2 \alpha^2 \gamma^2 \phi^2}{(1+n)(2+n)(3+n)} - \frac{12n^3 p^2 \pi^4 q^2 \alpha^2 \gamma^2 \phi^2}{(1+n)(2+n)(3+n)} \\
& + \frac{72np^2 \pi^4 q^2 \alpha^2 \gamma^2 v \phi^2}{(1+n)(2+n)(3+n)} + \frac{60n^2 p^2 \pi^4 q^2 \alpha^2 \gamma^2 v \phi^2}{(1+n)(2+n)(3+n)} + \frac{12n^3 p^2 \pi^4 q^2 \alpha^2 \gamma^2 v \phi^2}{(1+n)(2+n)(3+n)} \\
& - \frac{12p^2 \pi^4 q^2 \phi^2 E_r}{(1+n)(2+n)(3+n)} - \frac{6np^2 \pi^4 q^2 \phi^2 E_r}{(1+n)(2+n)(3+n)} - \frac{6n^2 p^2 \pi^4 q^2 \phi^2 E_r}{(1+n)(2+n)(3+n)} \\
& - \frac{72p^2 \pi^4 q^2 \alpha^2 \gamma^2 \phi^2 E_r}{(1+n)(2+n)(3+n)} - \frac{60np^2 \pi^4 q^2 \alpha^2 \gamma^2 \phi^2 E_r}{(1+n)(2+n)(3+n)} - \frac{12n^2 p^2 \pi^4 q^2 \alpha^2 \gamma^2 \phi^2 E_r}{(1+n)(2+n)(3+n)} \\
& + \frac{72p^2 \pi^4 q^2 \alpha^2 \gamma^2 v \phi^2 E_r}{(1+n)(2+n)(3+n)} + \frac{60np^2 \pi^4 q^2 \alpha^2 \gamma^2 v \phi^2 E_r}{(1+n)(2+n)(3+n)} + \frac{12n^2 p^2 \pi^4 q^2 \alpha^2 \gamma^2 v \phi^2 E_r}{(1+n)(2+n)(3+n)}
\end{aligned} \tag{A36}$$

$$\begin{aligned}
W_{33c} = & -\frac{8np^4 \pi^4}{(1+n)(2+n)(3+n)} - \frac{3n^2 p^4 \pi^4}{(1+n)(2+n)(3+n)} - \frac{n^3 p^4 \pi^4}{(1+n)(2+n)(3+n)} \\
& - \frac{36np^4 \pi^4 \alpha^2 \gamma^2}{(1+n)(2+n)(3+n)} - \frac{30n^2 p^4 \pi^4 \alpha^2 \gamma^2}{(1+n)(2+n)(3+n)} - \frac{6n^3 p^4 \pi^4 \alpha^2 \gamma^2}{(1+n)(2+n)(3+n)} \\
& + \frac{36np^4 \pi^4 \alpha^2 \gamma^2 v}{(1+n)(2+n)(3+n)} + \frac{30n^2 p^4 \pi^4 \alpha^2 \gamma^2 v}{(1+n)(2+n)(3+n)} + \frac{6n^3 p^4 \pi^4 \alpha^2 \gamma^2 v}{(1+n)(2+n)(3+n)} \\
& - \frac{6p^4 \pi^4 E_r}{(1+n)(2+n)(3+n)} - \frac{3np^4 \pi^4 E_r}{(1+n)(2+n)(3+n)} - \frac{3n^2 p^4 \pi^4 E_r}{(1+n)(2+n)(3+n)} \\
& - \frac{36p^4 \pi^4 \alpha^2 \gamma^2 E_r}{(1+n)(2+n)(3+n)} - \frac{30np^4 \pi^4 \alpha^2 \gamma^2 E_r}{(1+n)(2+n)(3+n)} - \frac{6n^2 p^4 \pi^4 \alpha^2 \gamma^2 E_r}{(1+n)(2+n)(3+n)} \\
& + \frac{36p^4 \pi^4 \alpha^2 \gamma^2 v E_r}{(1+n)(2+n)(3+n)} + \frac{30np^4 \pi^4 \alpha^2 \gamma^2 v E_r}{(1+n)(2+n)(3+n)} + \frac{6n^2 p^4 \pi^4 \alpha^2 \gamma^2 v E_r}{(1+n)(2+n)(3+n)}
\end{aligned} \tag{A37}$$